



UNIVERSITY OF LEEDS

This is a repository copy of *Oil production enhancement, asphaltene precipitation and permeability damage during CO<sub>2</sub>-SAG flooding of multi-layer sandstone reservoirs*.

White Rose Research Online URL for this paper:

<https://eprints.whiterose.ac.uk/183433/>

Version: Accepted Version

---

**Article:**

Wang, Q, Shen, J, Glover, PWJ [orcid.org/0000-0003-1715-5474](https://orcid.org/0000-0003-1715-5474) et al. (2 more authors) (2022) Oil production enhancement, asphaltene precipitation and permeability damage during CO<sub>2</sub>-SAG flooding of multi-layer sandstone reservoirs. *Journal of Petroleum Science and Engineering*, 212. 110241. ISSN 0920-4105

<https://doi.org/10.1016/j.petrol.2022.110241>

---

© 2022, Elsevier. This manuscript version is made available under the CC-BY-NC-ND 4.0 license <http://creativecommons.org/licenses/by-nc-nd/4.0/>.

**Reuse**

This article is distributed under the terms of the Creative Commons Attribution-NonCommercial-NoDerivs (CC BY-NC-ND) licence. This licence only allows you to download this work and share it with others as long as you credit the authors, but you can't change the article in any way or use it commercially. More information and the full terms of the licence here: <https://creativecommons.org/licenses/>

**Takedown**

If you consider content in White Rose Research Online to be in breach of UK law, please notify us by emailing [eprints@whiterose.ac.uk](mailto:eprints@whiterose.ac.uk) including the URL of the record and the reason for the withdrawal request.



[eprints@whiterose.ac.uk](mailto:eprints@whiterose.ac.uk)  
<https://eprints.whiterose.ac.uk/>

# Oil production enhancement, asphaltene precipitation and permeability damage during CO<sub>2</sub>-SAG flooding of multi-layer sandstone reservoirs

Qian Wang<sup>1\*</sup>, Jian Shen<sup>1</sup>, Paul W.J. Glover<sup>2</sup>, Piroska Lorinczi<sup>2</sup>, Wei Zhao<sup>3</sup>

<sup>1</sup>School of Resources and Geosciences, China University of Mining and Technology, Xuzhou, 221116, China

<sup>2</sup>School of Earth and Environment, University of Leeds, Leeds, LS2 9JT, UK

<sup>3</sup>China Petroleum Technology and Development Corporation, Beijing, 100028, China

**Abstract:** The process of CO<sub>2</sub>-SAG flooding involves conventional miscible CO<sub>2</sub> flooding until breakthrough (BT), followed by a period of CO<sub>2</sub> soaking or shut-in, and then a continuation of the miscible CO<sub>2</sub> flooding. The SAG process provides different improvement in the oil recovery for different positions of each layer in multilayer reservoirs, and has different effects on the distribution of pore throat blocking and adsorption of asphaltene to mineral surfaces. In this paper, both miscible CO<sub>2</sub>-SAG and conventional CO<sub>2</sub> flooding experiments have been carried out at reservoir conditions and on multi-layer systems composed of parallel connection of long cores. After CO<sub>2</sub>-SAG flooding oil recovery factors (RF) of the low, medium and high permeability cores were 7.7%, 8.3%, and 7.6% higher compared to the RFs after CO<sub>2</sub> flooding. The respective fractional oil production (FOP) of each long core were 10.6%, 27.7%, and 61.6% after CO<sub>2</sub>-SAG flooding, with less difference between each long core than CO<sub>2</sub> flooding. After CO<sub>2</sub> flooding, the permeability of the high permeability core at the injection end dropped by 24.5-25.8%, which is 5.5-14.3% higher than the value at the outlet. The permeability decrease due to CO<sub>2</sub>-SAG flooding was 0.7-9.7% higher than that due to CO<sub>2</sub> flooding, and the distribution of permeability decline is more homogeneous. The contribution of the total permeability decrease attributable to asphaltene particle blockage due to CO<sub>2</sub> flooding was 84.7-62.7%, 5.2-10.1% higher than that due to CO<sub>2</sub>-SAG flooding, gradually decreasing along the flow direction. Complex two phase flow of oil and gas is more likely to cause pore throat blockage instead of causing the adsorption of asphaltene precipitation.

30

31 **Keywords:** CO<sub>2</sub>-SAG flooding, multilayer reservoirs, asphaltene precipitation, blockage and  
32 absorption, permeability decline.

33

## 34 **Introduction**

35 The injection of CO<sub>2</sub> into reservoirs is a proven effective enhanced oil recovery (EOR)  
36 method<sup>[1-3]</sup>. Oil viscosity and interfacial tension reduction, volume swelling, light-hydrocarbon  
37 extraction during CO<sub>2</sub> flooding are all important effects which contribute to the EOR process<sup>[4-  
38 5]</sup>. Continuous miscible CO<sub>2</sub> flooding is a practical and efficient displacement technology<sup>[6]</sup>.  
39 Regrettably, conventional CO<sub>2</sub> injection suffers from flow instability and viscous fingering,  
40 and consequently, early CO<sub>2</sub> breakthrough<sup>[7]</sup>. Especially, most oil reservoirs are composed of a  
41 series of relatively layers with variable permeabilities. In these reservoirs, CO<sub>2</sub> breakthrough  
42 occurs first from layers of high permeability. The gas pathway is established through these high  
43 permeability layers, which results in a large volume of crude oil in lower permeability layers  
44 being by-passed and, consequently, unproduced<sup>[8-9]</sup>.

45

46 The CO<sub>2</sub>-soaking-alternating-gas flooding process (CO<sub>2</sub>-SAG) is a combination of  
47 conventional continuous miscible CO<sub>2</sub> flooding with a CO<sub>2</sub> soaking stage from the CO<sub>2</sub> huff-  
48 and-puff process<sup>[10]</sup>. In the first stage CO<sub>2</sub> is continuously injected into the reservoir in the same  
49 way as in the conventional miscible CO<sub>2</sub> process. The CO<sub>2</sub>-SAG process differs from  
50 conventional CO<sub>2</sub> flooding by being stopped at breakthrough. The second stage of the CO<sub>2</sub>-  
51 SAG process is a soaking period, in which both the injector and producer are shut in. During  
52 this period the injected CO<sub>2</sub> diffuses into the residual oil and water in the reservoir, accessing  
53 those fluids with which the gas was not in contact during the dynamic first stage of the process.  
54 The oil becomes larger in volume and significantly more mobile, allowing it to leave some of  
55 the smaller and more inaccessible pores and occupy instead the CO<sub>2</sub> saturated high permeability

56 channels opened up by the initial flooding in Stage 1 to CO<sub>2</sub> BT<sup>[11]</sup>. The third stage is another  
57 simple miscible CO<sub>2</sub> flood to displace and recover the residual oil that was freed in Stage 2<sup>[12]</sup>.

58

59 The CO<sub>2</sub>-SAG process results in better dissolution of CO<sub>2</sub> in crude oil than either the CO<sub>2</sub> huff-  
60 and-puff process, which depends only on the diffusion of molecular CO<sub>2</sub>, or conventional CO<sub>2</sub>  
61 flooding, where CO<sub>2</sub> only dissolves in the crude oil in direct dynamical contact with the flood  
62 front. The improved interaction between CO<sub>2</sub> and crude oil that occurs during the soaking  
63 process substantially promotes the miscibility of oil and CO<sub>2</sub>, and increases the CO<sub>2</sub>  
64 displacement efficiency during secondary CO<sub>2</sub> flooding, with higher CO<sub>2</sub> utilization efficiency  
65 and lower injection cost<sup>[13]</sup>.

66 No matter what kind of CO<sub>2</sub> flooding method is adopted, the CO<sub>2</sub> dissolution or light  
67 component stripping of crude oil perturbs crude oil thermodynamically, which promotes the  
68 precipitation and flocculation of asphaltenes<sup>[14-15]</sup>. A proportion of these particles of asphaltene  
69 become adsorbed onto mineral surfaces within the rock matrix altering the wettability and  
70 hence capillary properties and permeability of the rock. The remaining asphaltene agglomerates  
71 remain suspended in the fluid and are transported by the pore fluids until they become trapped  
72 in pores and pre throats leading to blockages. These blockages can result in extremely  
73 significant drops of permeability<sup>[16-17]</sup>.

74

75 Moreover, heterogeneity has a markedly important influence on the final efficacy of the CO<sub>2</sub>-  
76 SAG process<sup>[20]</sup>. In multilayer reservoirs the enhancement depends on the quality of the  
77 reservoir rock in a given layer and its position along the core as well as the proximity of other  
78 layers with different flow characteristics. Reservoir heterogeneity between layers with different  
79 permeability also affects the distribution and amount of reservoir damage after flooding<sup>[18-20]</sup>.

80 In addition, the adsorption and blockage of asphaltene precipitation cause different damage to  
81 the permeability at different locations within the reservoir, with different adsorption and  
82 blockage mechanisms<sup>[21]</sup>.

83

84 In order to formulate more targeted and effective measures in heterogeneous layered reservoir,  
85 as well as to prevent or reduce the damage to rock permeability caused by asphaltene  
86 precipitation, distinguishing the damage to permeability from blockage and adsorption is  
87 required. As a result, the quantification of the influence of the CO<sub>2</sub>-SAG process on oil recovery  
88 must also be balanced by any deleterious effect on permeability.

89  
90 There is a relatively small number of core-flooding experiments which have focused on the  
91 technical potential of CO<sub>2</sub>-SAG flooding. Nevertheless, they permit a number of key issues to  
92 be targeted for further study, such as CO<sub>2</sub> injection flow rate and pressure, the parameters which  
93 control the optimal CO<sub>2</sub> soaking period, the effect of water pre-flooding, cores with different  
94 permeability were subjected to CO<sub>2</sub>-SAG flooding experiments under different conditions<sup>[12,22]</sup>.  
95 We have carried out SAG flooding experiments on cores with similar permeability but different  
96 pore throat structures and single heterogeneous long cores, and studied the effects of pore  
97 structure and linear heterogeneity on the micro and macro crude oil production improvement  
98 of CO<sub>2</sub>-SAG flooding and the distribution of permeability damage<sup>[10,13]</sup>. Furthermore, there has  
99 been no previous study of the combined improvement in hydrocarbon recovery and progress of  
100 permeability damage in heterogeneous reservoirs consisting of multiple layers of rocks with  
101 different pore microstructures after both types of flooding. In particular, there is a lack of  
102 research on the distribution of asphaltene precipitation in the blocked and adsorbed state.

103  
104 In this paper, CO<sub>2</sub>-SAG and conventional CO<sub>2</sub> flooding have been carried out at reservoir  
105 conditions on two assemblages of three long cores with different permeability ,which are  
106 arranged in parallel in separate core holders and representing three parallel layers in a reservoir.  
107 The porosity and permeability between the analogue cores in the two assemblages are almost  
108 the same. The results presented in this paper cover the comparison of the efficiency of  
109 miscible CO<sub>2</sub>-SAG flooding with simple miscible CO<sub>2</sub> flooding, focusing on (i) fluid  
110 displacement, (ii) oil production enhancement and its distribution, (iii) the distribution of  
111 permeability damage due to the blockage and adsorption of asphaltene precipitation. The

112 progress and extent of each effect has been compared across each of the three different pore  
113 microstructures (layers). The results furnish information allowing the advantages,  
114 disadvantages, benefits and risks of different CO<sub>2</sub> flooding methodologies to be judged in  
115 heterogeneous layered reservoir, especially with regard to reservoir damage and the saturation  
116 of residual oil.

117

## 118 **Methodology**

### 119 **Materials**

120 A crude oil sample taken from the Jilin oilfield in the northeast of China and analyzed to obtain  
121 its composition(table 1). The compositional results were used to synthesize a live oil, which  
122 was subsequently used in all of the experiments. The proportion of *n*-C<sub>5</sub>-insoluble asphaltene  
123 in the Jilin oil sample was 3.18 wt% <sup>[10]</sup>. The minimum miscible pressure of the CO<sub>2</sub>-crude oil  
124 system was measured by slim-tube apparatus and discovered to be 20.6±0.4 MPa at  
125 90±0.1°C<sup>[10]</sup>. The relationship between asphaltene precipitation and the crude oil CO<sub>2</sub>  
126 concentration has also been measured previously<sup>[10]</sup>, asphaltenes begin to precipitate from crude  
127 oil at a dissolved CO<sub>2</sub> concentration of 29.5mol%, and completely precipitate at 60 mol%. as  
128 well as being predicted using the Flory-Huggins model<sup>[15]</sup>. We note that the measured and  
129 predicted values differ by <5%. The CO<sub>2</sub> solubility in the Jilin crude oil is 68.3 mol% and the  
130 oil viscosity decreases from 2.11 mPa·s (0 mol% CO<sub>2</sub>) to 0.62 mPa·s (68.3 mol% CO<sub>2</sub>) at 23  
131 MPa and 90°C <sup>[10]</sup>.

132

133 This study used two types of brine. The first was prepared to the compositional recipe given in  
 134 Table 2<sup>[10]</sup>. The second was prepared from the same compositional recipe but with the addition  
 135 of Mn<sup>2+</sup>, which was added to remove the signal arising from water when making nuclear  
 136 magnetic resonance (NMR) measurements in order to obtain the oil distribution in the core<sup>[23]</sup>.

137

138 **Table 1.** Basic physical properties of live oil together with its compositional analysis (n-C5  
 139 insoluble asphaltene content =3.18 wt%).

Property		Value			
Density (g/cm <sup>3</sup> )		0.731±0.002 (90°C)			
Viscosity (mPa·s)		2.11±0.04 (90°C)			
Solution gas-oil ratio (m <sup>3</sup> /m <sup>3</sup> )		44.7			
Bubble point pressure (MPa)		6.95			
Composition					
Carbon number	wt%	Carbon number	wt%	Carbon number	wt%
CO <sub>2</sub>	0.053	C9	4.640	C21	2.16
N <sub>2</sub>	0.422	C10	4.531	C22	2.304
C1	1.741	C11	3.947	C23	2.104
C2	1.126	C12	3.615	C24	2.088
C3	0.998	C13	3.261	C25	1.948
<i>i</i> C4	0.178	C14	2.908	C26	1.872
<i>n</i> C4	0.525	C15	2.633	C27	1.896
<i>i</i> C5	0.942	C16	3.615	C28	1.766
<i>n</i> C5	0.353	C17	3.567	C29	1.882
C6	1.365	C18	3.222	C30+	26.363
C7	2.52	C19	2.484	<b>Total</b>	<b>100</b>
C8	4.409	C20	2.563		

140

141

**Table 2.** Physicochemical properties of the reservoir brine.

Item	Value
Density (g/cm <sup>3</sup> )	1.005
Viscosity at 25°C (mPa·s)	1.02
pH	7.04
K <sup>+</sup> (mg/L)	1473
Na <sup>+</sup> (mg/L)	3546
Ca <sup>2+</sup> (mg/L)	116

Mg <sup>2+</sup> (mg/L)	33
Cl <sup>-</sup> (mg/L)	5261
SO <sub>4</sub> <sup>2-</sup> (mg/L)	1288
HCO <sub>3</sub> <sup>-</sup> (mg/L)	1559
TDS (mg/L)	13276

142 TDS = Total dissolved solids.

143

144 The artificial long cores used in the tests are composed of epoxy resin and quartz sand with  
 145 different grain size distributions, which were cold isostatically pressed<sup>[24]</sup> (Figure 1). The  
 146 petrophysical characteristics of these core samples are shown in Table 3. The long cores are  
 147 approximately homogeneous (the difference between the porosity or permeability at any  
 148 position in the sample is within  $\pm 2.7\%$  and  $\pm 3.3\%$  of the mean porosity or permeability value  
 149 for the core, respectively). Three cores with different permeabilities and porosities were used  
 150 in a triad to represent three reservoir layers with different permeabilities. Consequently, though  
 151 the results discussed in this paper refer to three different cores, they represent analogue layers  
 152 in a reservoir.

153



154

155

**Figure 1.** Schematic diagram of an artificial homogeneous long core.

156

157

**Table 3.** Fundamental characteristics of the core samples used in this work.

Flooding method	Core number	Length (cm)	Diameter (cm)	Permeability (mD)	Porosity (%)
	H <sub>1</sub>	50.2	2.52	25.7	14.4
CO <sub>2</sub> flooding	H <sub>2</sub>	50.4	2.52	51.8	16.7
	H <sub>3</sub>	50.1	2.52	75.7	19.2



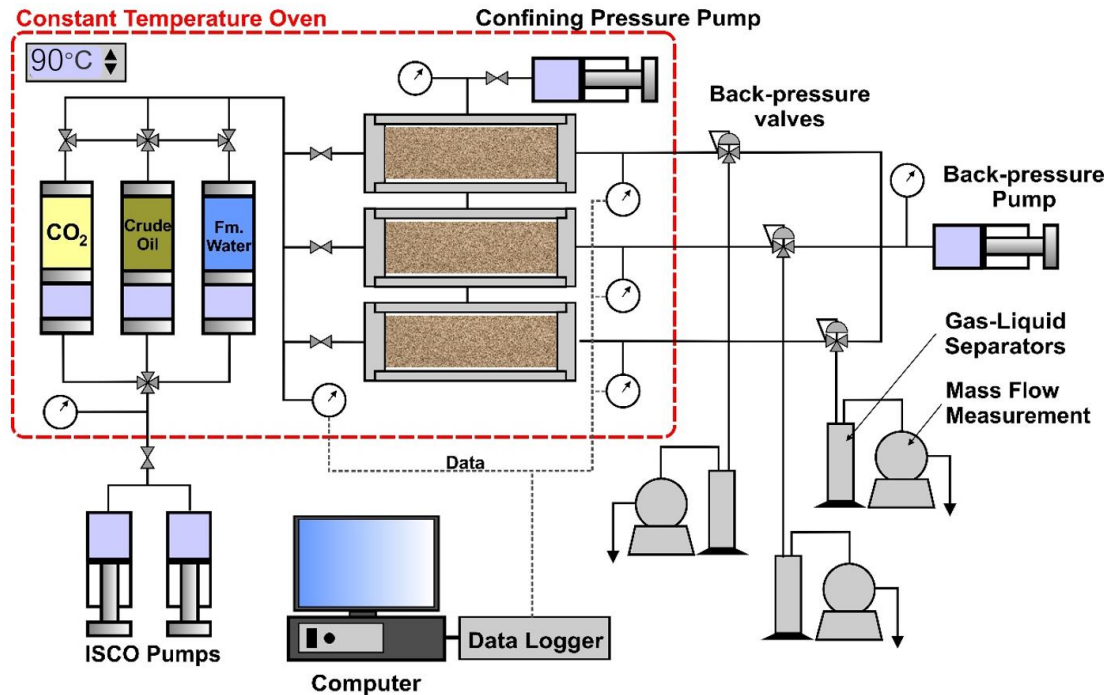
CO <sub>2</sub> -SAG flooding	J <sub>1</sub>	50.3	2.52	26.3	14.1
	J <sub>2</sub>	50.1	2.53	50.1	17.1
	J <sub>3</sub>	49.8	2.52	76.2	18.8

158

159 **Core-flooding tests**

160 The flow diagram of core flooding apparatus used in this study is shown in Figure 2. In this  
 161 arrangement, three core holders (Hongda, China,  $L=75$  cm,  $T_{\max}=130^{\circ}\text{C}$ ,  $P_{\max}=80$  MPa) are  
 162 positioned horizontally and connected in parallel in order to simulate a multilayer reservoir.  
 163 Process fluids (CO<sub>2</sub>, live oil, and brine with MnCl<sub>2</sub> (Mn<sup>2+</sup>, 15g/L)) were delivered  
 164 independently to the cores (Figure 2) using three separate high-pressure cylinders (Hongda,  
 165 China;  $T_{\max}=130^{\circ}\text{C}$ ;  $P_{\max}=80$  MPa). The temperature of all core holders and tanks was ensured  
 166 by placing them in an oven (Hongda, China;  $T_{\max}=120.0\pm 0.1^{\circ}\text{C}$ ). Displacement of CO<sub>2</sub>, crude  
 167 oil, and brine into the multilayer core system was implemented using a dual ISCO syringe  
 168 pump. A second pump was used to apply a constant confining pressure. A third pump was used  
 169 together with three back pressure valves to ensure that the backpressure was controlled and  
 170 constant. A set of gas-liquid separators and mass flow meters was used to measure the fluids  
 171 produced from each core. All data, including pressure and flow data were collected and logged  
 172 using a computer.

173



174

175

**Figure 2.** Schematic diagram of flooding experiments.

176

177 Conventional miscible CO<sub>2</sub> core flooding tests were carried out on cores H<sub>1</sub>, H<sub>2</sub> and H<sub>3</sub> in the  
 178 following two steps.

- 179 (1) The oven and the core-flooding flow rig it contains was raised to 90°C and kept at this  
 180 temperature for 24 hours to ensure a constant starting temperature in all parts of the  
 181 apparatus inside the oven and all process fluids. Cores H<sub>1</sub>, H<sub>2</sub> and H<sub>3</sub> were cleaned and  
 182 dried, and then placed in their core holders. Each core was subjected to separate evacuation  
 183 for 24 hours. Brine with MnCl<sub>2</sub> was injected into each core, separately. A maximum of 30  
 184 HCPV of crude oil was then pumped into each core separately in order to attain the connate  
 185 water saturations ( $S_{wc}$ ) and initial oil saturations ( $S_{oi}$ ) in each core. Subsequently, all core  
 186 holders were left undisturbed for 24 hours in order to obtain equilibrium at reservoir  
 187 conditions (90°C, 23MPa).
- 188 (2) A constant flow of CO<sub>2</sub> was injected at a rate of 18 cm<sup>3</sup>/h (This injection rate is based on  
 189 the oilfield injection rate and the previous experiments<sup>[10]</sup>. This rate will not lead to a rapid  
 190 breakthrough of CO<sub>2</sub> BT, but a higher oil RF.) into all three cores at the same time from

191 the same inlet and at the same input pressure. The produced fluids from each core were  
192 collected and measured individually but at the same output pressure (23 MPa) using the  
193 back pressure pump and back pressure valves on each output line. The flow of CO<sub>2</sub> was  
194 stopped when there was no further oil production from the multilayer system. Steps (1)  
195 and (2) represent the core-flooding experiment using the conventional miscible CO<sub>2</sub>  
196 flooding process.

197  
198 The miscible CO<sub>2</sub>-SAG core flooding tests were carried out on cores J<sub>1</sub>, J<sub>2</sub>, J<sub>3</sub> using the  
199 following four steps.

200 (3) Step (1) was repeated, but using cores J<sub>1</sub>, J<sub>2</sub>, J<sub>3</sub>.

201 (4) Step (2) was conducted on the cores J<sub>1</sub>, J<sub>2</sub>, J<sub>3</sub>, but stopping the core-flood as soon as CO<sub>2</sub>  
202 breakthrough (BT) occurred. This CO<sub>2</sub> injection will be called the primary injection.

203 (5) All three core holders were isolated during the CO<sub>2</sub> soaking stage by closing all input and  
204 output valves. The length of time for this shut is a critical parameter which is discussed  
205 later in the paper.

206 (6) The input and output valves were reopened, and CO<sub>2</sub> injection was recommenced into all  
207 three cores at a constant flow rate of at 18 cm<sup>3</sup>/h as in Step (4). This secondary CO<sub>2</sub> flood  
208 was continued until no further crude oil was produced.

209 The fluid volumes, injection pressures and production pressures and were monitored and  
210 recorded continuously during the entire flooding process. The asphaltene content of all  
211 produced oil was also measured.

212

### 213 Post-flooding tests

214 All the long cores were divided into 10 core plugs with the same length after flooding, the  
215 resulting short cores were subjected to NMR testing (Mini-MR, Niumag, China) to obtain the  
216 residual oil distribution by transverse relaxation time (T<sub>2</sub>) spectrum analysis.

217

218 Asphaltene is soluble in aromatic hydrocarbons but not in alkanes. Other components of crude  
219 oil are soluble in alkanes. Consequently, *n*-heptane can be used to clean cores of their non-  
220 asphaltene oleic components<sup>[25]</sup>. In this work, the short cores were cleaned with *n*-heptane using  
221 the Soxhlet method (Soxhlet Extractor SXT-02, Shanghai Pingxuan Scientific Instrument CO.,  
222 Ltd., China) which removed all oleic fluids remaining in the cores after flooding, but leaving  
223 the asphaltene precipitation blocking pore throats and adsorbed to pore walls. Methanol was  
224 used to remove any aqueous fluids remaining after the floods. Subsequently, all of the short  
225 cores were dried. Their gas permeability was then measured. This permeability was the  
226 permeability that had been affected by asphaltene precipitation both blocking pore throats and  
227 due to adsorption to mineral surfaces.

228

229 It should be noted that due to the non-polar nature of cyclohexane on asphaltene dissolution,  
230 cyclohexane reversal flooding can remove the asphaltene blocking pore throats. By contrast,  
231 reverse flooding using toluene can remove any asphaltene adsorbed on mineral surfaces.  
232 Cyclohexane reverse flooding was performed (flow rate =30 cm<sup>3</sup>/h until a stable differential  
233 pressure was sustained) to measure any formation damage that had accrued from the  
234 mechanical blocking of pores and pore throats<sup>[15]</sup>. It was found that this process removed  
235 asphaltene due to mechanical blockage of pore throats in all cores. The cores were then cleaned,  
236 allowing the decline in permeability decline associated with asphaltene pore throat blockage to  
237 be quantified.

238

239 Subsequently, the cores were subjected to reverse flooding with toluene<sup>[16]</sup>, in order to remove  
240 adsorbed asphaltenes that could not be removed with cyclohexane. The cores were then cleaned  
241 again, and the permeability was remeasured in order to obtain the permeability decline due to  
242 the adsorption of asphaltenes directly to mineral surfaces.

243

244 **Results and Discussion**

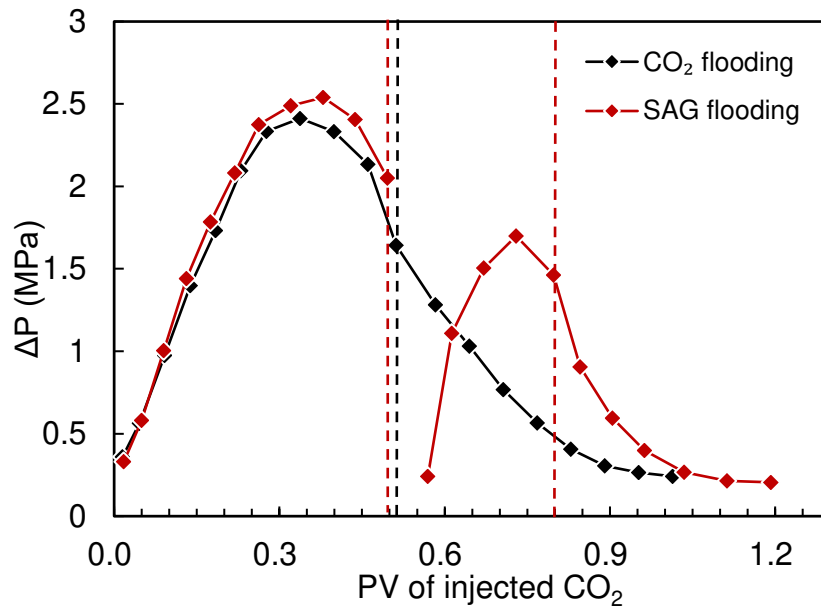
245 Differential pressures ( $\Delta P$ )

246 Figure 3 shows that the dynamic trend of the  $\Delta P$  values during CO<sub>2</sub> and SAG flooding are very  
247 similar during the continuous CO<sub>2</sub> injection before CO<sub>2</sub> BT. The similar behavior is attributed  
248 to the matched physical properties of the two groups of cores composing the three-layer system  
249 (see Table 3), and suggests that their similar petrophysical properties result in similar  
250 distributions of fluids at the start of the experiment and progressively during initial CO<sub>2</sub>  
251 flooding.

252

253 In the SAG flooding process, the CO<sub>2</sub> soaking stage was started after the CO<sub>2</sub> BT (occurring at  
254 0.4961 PV), and then the secondary CO<sub>2</sub> flooding was performed (until 1.192 PV). During the  
255 CO<sub>2</sub> soaking stage, the crude oil that had not previously interacted sufficiently with CO<sub>2</sub> had  
256 the opportunity to adsorb CO<sub>2</sub>. As a consequence, the volume of this crude oil expanded and  
257 its viscosity decreased, leading to the redistribution of fluids within the pores. The saturation  
258 of the oil in the pores that had composed the well-connected and larger pore size gas channels  
259 formed by the initial CO<sub>2</sub> flooding increased. Consequently, the displacement resistance of  
260 SAG secondary flooding was greater than that during CO<sub>2</sub> flooding at same injected CO<sub>2</sub>  
261 volume, and less than that before CO<sub>2</sub> BT. The secondary CO<sub>2</sub> BT occurred more quickly due  
262 to the higher gas saturation and lower oil viscosity in the rock at the beginning of the secondary  
263 flooding. It is worth noting that the CO<sub>2</sub> BT only occurs in the high permeability layers during  
264 CO<sub>2</sub> flooding and SAG flooding. There is no obvious CO<sub>2</sub> BT in the medium and low  
265 permeability layers, and the displacement front of CO<sub>2</sub> flooding does not advance to the outlet  
266 end.

267



268

269 **Figure 3.** Measured differential pressure ( $\Delta P$ ) during CO<sub>2</sub> flooding and SAG flooding.  
 270 Vertical dashed lines show CO<sub>2</sub> BT for each flood.

271

272 Pressure decay during the CO<sub>2</sub>-soaking process

273 Figure 4 shows that the core fluid pressure declines rapidly as soon as the CO<sub>2</sub>-soaking process  
 274 begins, becoming progressively slower. The pressure-time curve can be approximated by a  
 275 power-law, fits of which are also shown in the figure. This behavior arises from (i) dissolution  
 276 of gas in the oil near the gas-oil interface, and (ii) gas diffusion deeper into the oil. Both of  
 277 these processes depend on the partial pressure of gas already in the oil. As a result, dissolution  
 278 becomes progressively less efficient until a steady-state is reached<sup>[26-27]</sup>.

279

280 In our case, the cores were soaked in brine and cleaned before the laboratory experiments were  
 281 carried out. This process makes the cores water-wet, with water preferentially coating the  
 282 surfaces of rock grains and completely filling the smallest pores. By contrast, crude oil and CO<sub>2</sub>  
 283 are non-wetting phases. Such non-wetting phases occupy the center of large and medium-sized  
 284 pores and pore throats as far from the mineral surfaces as possible. The injected CO<sub>2</sub> prefers to  
 285 be in contact with the crude oil in the center of the large pores and throats. Under these  
 286 conditions, we expect that the initial swift pressure drop occurs as the result of efficient

287 dissolution of gas in oil with which it is in direct contact. Once the partial pressure of CO<sub>2</sub>  
288 within this oil approaches saturation, further decay will be controlled by gas diffusion within  
289 the oil<sup>[28-29]</sup>. However, gas diffusion through oil in small pores and between pores with small  
290 pore throats will be slowed down by the greater tortuosity of the oil pathways through which  
291 the gas must diffuse. The process of gas diffusion is therefore relatively slow<sup>[30-31]</sup>. As a  
292 consequence, there exists an optimal soaking time ( $T_c$ ) at which the dissolution of CO<sub>2</sub> in oil is  
293 maximized, allowing the oil to swell and develop greater mobility, while avoiding slow  
294 pressure decay stage. This  $T_c$  is exhibited as an inflexion in the pressure decay.

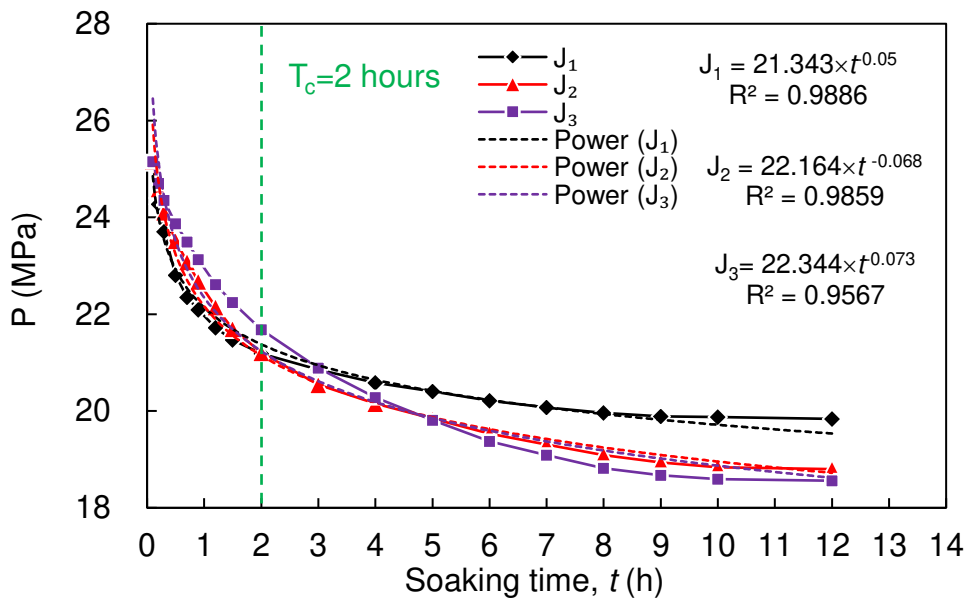
295

296 The determination of the  $T_c$  value can improve the efficiency of SAG flooding in oilfield  
297 development. Usually, a pressure decay rate threshold value is established, and the soaking  
298 stage is stopped when the decay rate is lower than this value. For example, in the results of this  
299 experiment, when the pressure decay rate in the core J<sub>3</sub> is lower than 1 MPa/h (the pressure  
300 decay of J<sub>3</sub> is the slowest among the three cores),  $T_c=2$  h. When threshold value is applied in  
301 oilfield development, the threshold value should be determined according to the specific  
302 characteristics of the reservoir and the characteristics of pressure attenuation.

303

304 The greater the permeability, the greater the pressure decay rate. This is due to there being less  
305 residual oil in the high permeability core at the beginning of the soaking stage, as well as to the  
306 fact that the higher the CO<sub>2</sub> saturation, the larger the contact area between CO<sub>2</sub> and the fluid in  
307 the core, and the better connectivity between the pores, the faster the diffusion of CO<sub>2</sub> in the  
308 fluid in high-permeability core. By contrast, the lower the core permeability, the poorer the  
309 connectivity between the pores, the lower the pressure decay rate, and the lower the final  
310 equilibrium pressure, the greater the  $T_c$  value. Such a scenario is an indicator that lower  
311 permeability cores require longer soaking times in order for the process to be effective.

312



313

314 **Figure 4.** Measured CO<sub>2</sub> pressure in the core plugs with respect to soaking time  $t$ , with best-  
 315 fit power laws.

316

317 Oil recovery and produced fluids

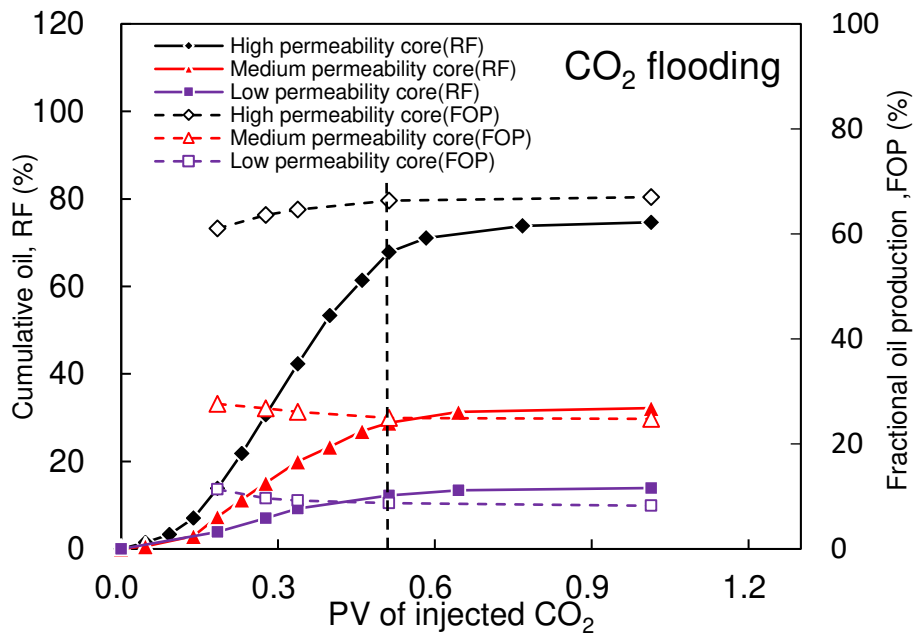
318 Figure 5 and Table 4 show that the dynamic production of crude oil during the two flooding  
 319 processes had similar characteristics up until CO<sub>2</sub> BT. The high-permeability layer had the  
 320 highest oil RF as well as the fastest increase in RF. The fractional oil production (FOP) of high  
 321 permeability layer is the largest, and gradually increases, while the FOP of medium and low  
 322 permeability layers decreases gradually. This is because the high permeability layer presents  
 323 the smallest capillary resistance, the resistance of CO<sub>2</sub> flooding is small, and as the  
 324 displacement front advances faster in the high permeability layer, this displacement resistance  
 325 becomes smaller<sup>[32]</sup>. The difference in displacement resistance between layers with smaller  
 326 permeabilities is greater. A larger proportion of injected CO<sub>2</sub> enters the high-permeability layer.

327

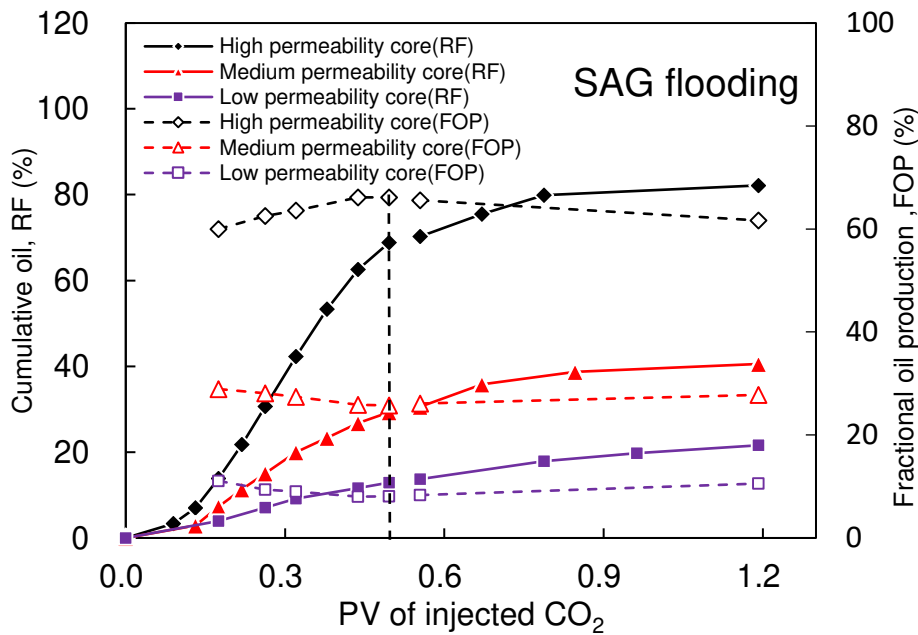
328 It is worth noting that there is a large difference between the ratio of the FOP of each layer  
 329 (67:25:8) and the ratio of the initial permeability (75:52:26), which means that a relatively small  
 330 difference in initial permeability would result in a huge difference in the FOP. In other words,  
 331 the influence of the initial permeability difference on the oil production effect is magnified



332 upon CO<sub>2</sub> injection. The oil RF of the high, medium and low cores increased little (by 6.8%,  
 333 3.4%, and 1.7%, respectively) after CO<sub>2</sub> BT during CO<sub>2</sub> flooding, even after a large volume of  
 334 CO<sub>2</sub> is continuously injected (Table 4). The oil production after CO<sub>2</sub> BT mainly comes from  
 335 high permeability layers. The oil production at this time depends mainly on the extraction of  
 336 CO<sub>2</sub> on oil, and the utilization efficiency of CO<sub>2</sub> is very poor<sup>[33]</sup>.  
 337



338



339

340 **Figure 5.** The cumulative oil RF and FOP of each long core. The vertical dashed line shows  
 341 the CO<sub>2</sub> BT at the end of the preliminary flood.

342

343 **Table 4.** Oil RF and FOP of each long core.

Flooding method	Timing	Oil RF %			Oil FOP %		
		High	Medium	Low	High	Medium	Low
Simple CO <sub>2</sub>	At CO <sub>2</sub> BT	67.8	28.8	12.2	66.4	24.9	8.7
	At flooding end	74.6	32.2	13.9	67	24.8	8.2
	$\Delta RF_1 \backslash \Delta FOP_1$	6.8	3.4	1.7	0.6	-0.1	-0.5
SAG	At CO <sub>2</sub> BT	68.9	29.4	12.9	66.2	25.7	8.1
	At flooding end	82.2	40.5	21.6	61.6	27.7	10.6
	$\Delta RF_1 \backslash \Delta FOP_1$	13.3	11.1	8.7	-4.6	2	2.5
SAG-Simple CO <sub>2</sub>	$\Delta RF \backslash \Delta FOP$	7.6	8.3	7.7	-5.4	2.9	2.4

344  $\Delta RF_1$  = Oil RF at flooding end - Oil RF at CO<sub>2</sub> BT

345  $\Delta FOP_1$  = Oil FOP at flooding end - Oil FOP at CO<sub>2</sub> BT

346  $\Delta RF$  = Oil RF at flooding end (SAG) - Oil RF at flooding end (Simple CO<sub>2</sub>)

347  $\Delta FOP$  = Oil FOP at flooding end (SAG) - Oil FOP at flooding end (Simple CO<sub>2</sub>)

348

349 During the secondary flooding process after the soaking stage in SAG flooding, the cumulative  
 350 recovery of each layer continued to increase, and the increased RF was 13.3%, 11.1%, and  
 351 8.7%, respectively (Table 4). Compared with CO<sub>2</sub> flooding, the medium and low permeability  
 352 cores attained relatively higher improvements in oil production, while the FOP of these layers  
 353 also increased after CO<sub>2</sub> BT. This is due to the soaking stage alleviating the problem of  
 354 inadequate contact between CO<sub>2</sub> and crude oil in the low and medium permeability layers. We  
 355 observe, particularly, that the high permeability layer has the best oil production improvement  
 356 after the soaking stage, while the FOP is reduced, indicating strongly that SAG not only  
 357 improves effectively the RF of the overall multi-layer system, but can also improve effectively  
 358 the oil production in low and medium permeability layers, reducing the difference in oil  
 359 production in each layer caused by the difference in initial permeability.

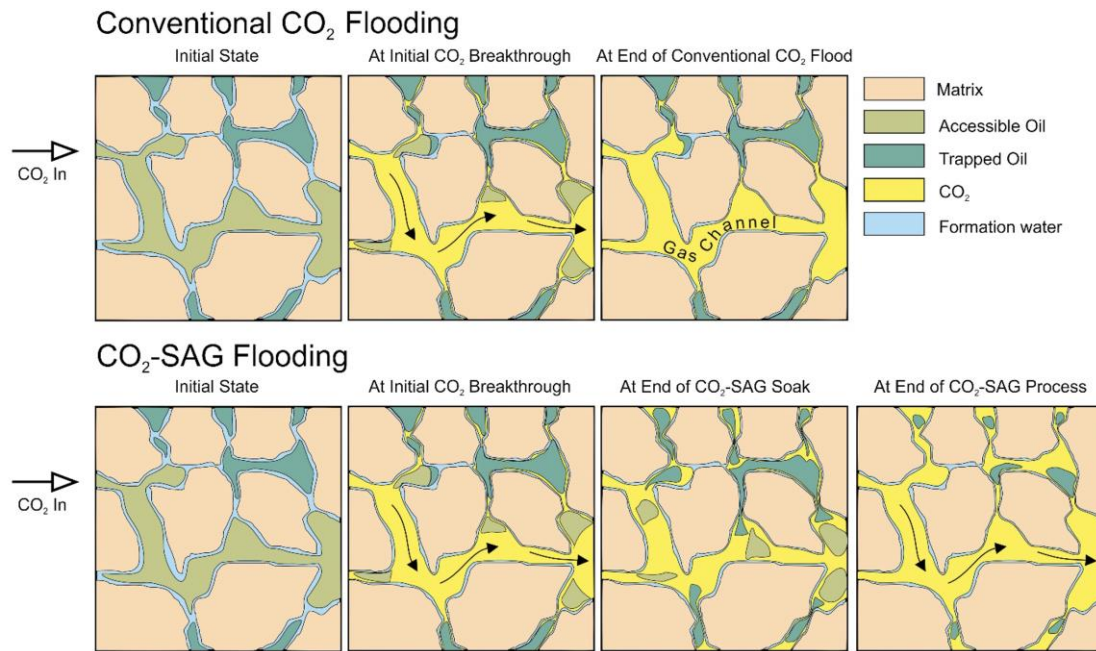
360

361 We found that the final oil RF of each layer of SAG flooding is 7.6%, 8.3%, and 7.7% higher  
362 than that of CO<sub>2</sub> flooding, i.e., approximately the same improvement for all of the layers,  
363 irrespective of their petrophysical properties (Table 4). Moreover, the difference in the FOP of  
364 each long core is, relatively speaking, smaller, which indicates that in the multi-layer reservoirs  
365 with different permeability CO<sub>2</sub>-SAG flooding is generally more effective than miscible CO<sub>2</sub>  
366 flooding in displacing oil, helping to tap the oil production potential of medium and low  
367 permeability layers.

368

369 Figure 6 shows the progression of the conventional CO<sub>2</sub> flooding process and the CO<sub>2</sub>-SAG  
370 flooding process. In both cases the initial state is shown on the left-hand side of the figure and  
371 injected CO<sub>2</sub> flows from left to right. The figure does not include changes due to asphaltene  
372 precipitation or pore blocking. The rock is assumed to be water-wet, and formation water is  
373 shown in blue. Oil is shown in two shades of green, according to whether it is accessible or  
374 trapped. For the purposes of this discussion ‘accessible oil’ is that which is mobile under normal  
375 CO<sub>2</sub> flooding conditions. This implies that the fluid pressure differences during flooding are  
376 greater than the capillary pressures retaining the oil in the pores, and further implies that  
377 accessible oil is to be found in the larger pores, and these pores are also linked by larger pore  
378 throats. By contrast, ‘trapped oil’ is that which occupies the smaller pores or pores only  
379 accessed by small pore throats. These oil accumulations are subjected to capillary pressures  
380 which are too high for them to be moved by the normal process of CO<sub>2</sub> flooding.

381



382

383 **Figure 6.** The progression of conventional CO<sub>2</sub> flooding and CO<sub>2</sub>-SAG flooding processes

384

exemplified using a microstructural/microfluidic model.

385

386 In the case of conventional CO<sub>2</sub> flooding process, injected CO<sub>2</sub> is not the wetting fluid. It  
 387 preferentially moves through pores with lower capillary pressures, either displacing oil or  
 388 occupying space between the oil and undisplaced oil. Since CO<sub>2</sub> has a much lower density and  
 389 viscosity than either oil or water, it is able to penetrate into small pores, even if it has little  
 390 ability to displace the oil from them. Consequently, by the time the CO<sub>2</sub> has broken through  
 391 (centre top panel of the Figure 6), there are three observations (i) CO<sub>2</sub> has displaced (and  
 392 produced) a large proportion of the accessible oil in the large pores, (ii) the flooding pathway  
 393 now predominantly contains gas, and this gas channel has a high permeability, which by-passes  
 394 oil in the remainder of the rock, and (iii) a small amount of residual accessible oil exists, for  
 395 which production depends on a marginal interplay between flooding pressures and the capillary  
 396 pressure. If flooding progresses after breakthrough, these final accumulations of oil will be  
 397 eventually produced (top left panel of the Figure 6).

398

399 In the case of CO<sub>2</sub>-SAG flooding, the story up until CO<sub>2</sub> breakthrough is the same as described  
 400 previously. During the soaking procedure, the remaining accessible and trapped oil undergo

401 two changes. First, the oil expands as CO<sub>2</sub> dissolves in the oil. The limited space in pores  
402 implies that some of the oil moves in response the subsequently increased fluid pressures.  
403 Second, solution of CO<sub>2</sub> in the oil also reduces the oil viscosity, making it more mobile. The  
404 result of these two effects results in the remaining accessible oil and some of the trapped oil  
405 extruding towards and into the high permeability gas channel. This situation is shown in the  
406 bottom third panel from the left. The presence of the CO<sub>2</sub> around the oil has changed its  
407 properties and brings the oil towards the high permeability channel. The promotion of oil RF  
408 by the miscible effect requires a certain amount of time and space for the interaction of CO<sub>2</sub>  
409 and crude oil, the soaking stage provides longer time of interaction. The second CO<sub>2</sub> flood is  
410 now capable of producing the more mobile extruded oil (bottom right-hand panel in the Figure  
411 6).

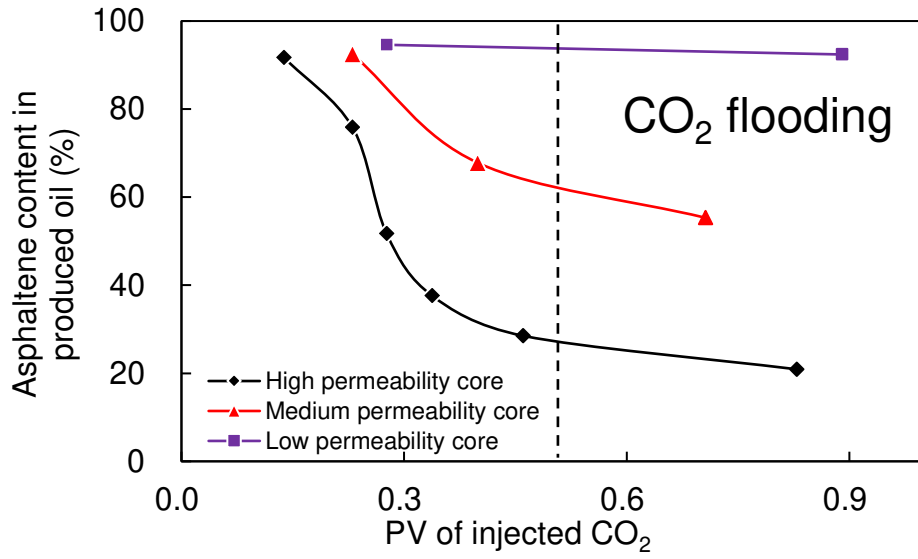
412

413 The asphaltene content of the produced crude oil decreases rapidly before CO<sub>2</sub> BT, as shown  
414 in Figure 7, with the production of crude oil, while the asphaltene content in the produced oil  
415 in the initial stage remained at 90%, and this part of the crude oil hardly came into contact with  
416 the injected CO<sub>2</sub>. There is an increase in the CO<sub>2</sub> dissolved in the crude oil as the displacement  
417 front progresses, which leads to increased asphaltene precipitation in the core and less  
418 asphaltene in the produced oil.

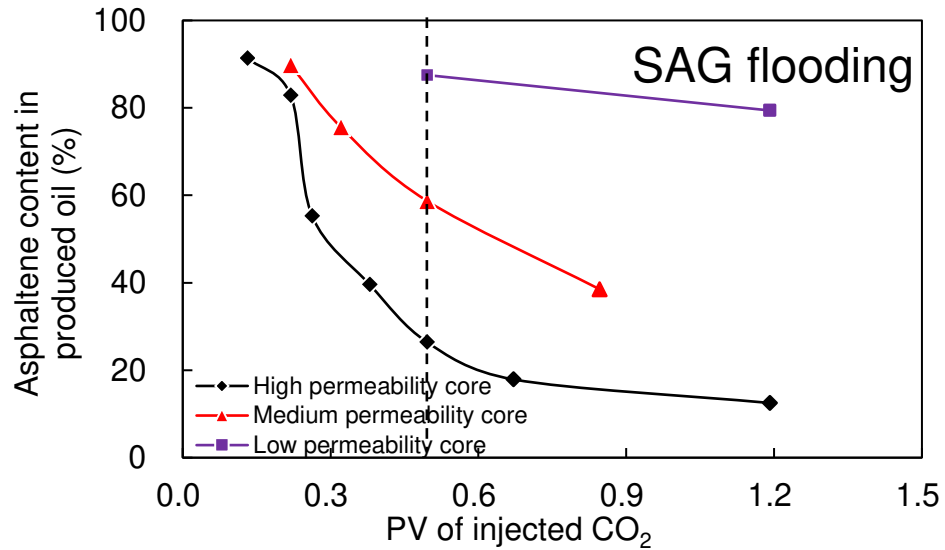
419

420 The asphaltene content of the produced oil after soaking was found to be smaller than that for  
421 miscible CO<sub>2</sub> flooding at the same amount of injected CO<sub>2</sub>. This may be ascribed to the larger  
422 amounts of CO<sub>2</sub> dissolved in the residual oil as a result of the soaking process, resulting in  
423 greater asphaltene precipitation, more asphaltene are deposited in the core during SAG  
424 flooding.

425



426



427

428 **Figure 7.** Asphaltene content in produced oil and PV of injected CO<sub>2</sub> during flooding.

429

430 Oil RF distribution

431 The NMR spectrometry provides the  $T_2$  relaxation time signal amplitude of the oil in each short  
 432 core plug (long cores are cut equally) after the experiments<sup>[34]</sup>. The oil RF of the cores at  
 433 different locations was calculated according to the volume of produced oil, saturated oil, and  
 434 the total intensity of the residual oil signal amplitude (Figure 8).

435

436 The oil RFs in the high permeability long core after conventional CO<sub>2</sub> flooding (Figure 8 upper  
437 panel) decreases gently along the injection direction. However, the oil RFs towards the middle  
438 ( $L=22-27$  cm) of the medium permeability layer exhibits a large variation, and the oil RF  
439 distribution along the injection direction is divided into two parts with gradual decrease, which  
440 may be attributed to the displacement front staying in this part of the rock ( $L=22-27$  cm) rather  
441 than advancing to the outlet at the end of the displacement by the development of fingering  
442 sufficient to ensure at least one gas channel breaks through. The same observation occurs at  $L$   
443  $=12-17$  cm in the low permeability long core, but this variation is smaller. For the medium and  
444 low permeability cores there is little variation of the oil RF in the latter half of the core, implying  
445 that the crude oil in the core with  $L > 17$  cm is not driven directly by CO<sub>2</sub>. Compared with the  
446 medium permeability long core, the displacement front in the low permeability long core is  
447 closer to the injection end.

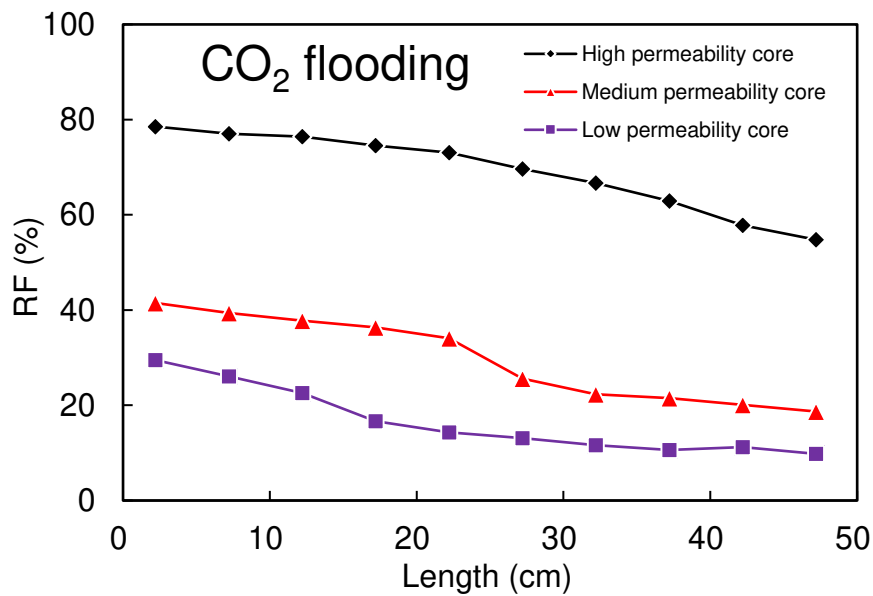
448

449 For CO<sub>2</sub>-SAG flooding, the oil RFs in each long core is large than that after conventional CO<sub>2</sub>  
450 flooding (Figure 9 lower panel). The curve variation ( $L =17-32$  cm) also appears in the high  
451 permeability layer. However, the soaking stage causes this variation to become flat, but the  
452 variation range becomes larger. There are two trends in the distribution of oil RF in high  
453 permeability layer. The pattern of oil RF in the rocks towards the injection end is relatively  
454 uniform, and varies little. The amount of oil RF near the outlet end shows an obvious gradual  
455 downward trend along the injection direction, and shows that the soaking process improves the  
456 efficiency of the residual oil at the injection end and middle being driven out during the  
457 secondary displacement process.

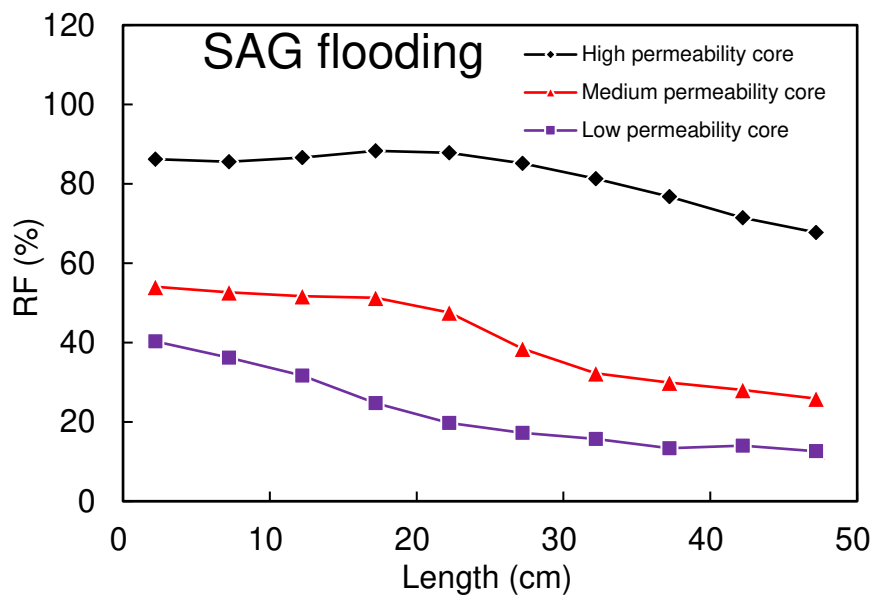
458

459 If the position of the displacement front in the same permeability core after CO<sub>2</sub> flooding is  
460 compared to that after SAG flooding, we observe that the displacement front in the low and  
461 medium permeability layers is not advanced significantly during secondary flooding as a result  
462 of the soaking stage. The soaking does not significantly expand the CO<sub>2</sub> swept volume, but

463 only enhances the CO<sub>2</sub> displacement effect in the core pores that have been swept by CO<sub>2</sub> before  
 464 CO<sub>2</sub> BT.  
 465



466



467

468 **Figure 8.** Oil recovery calculated according to the signal amplitude in  $T_2$  spectrum by NMR  
 469 tests along the cores.

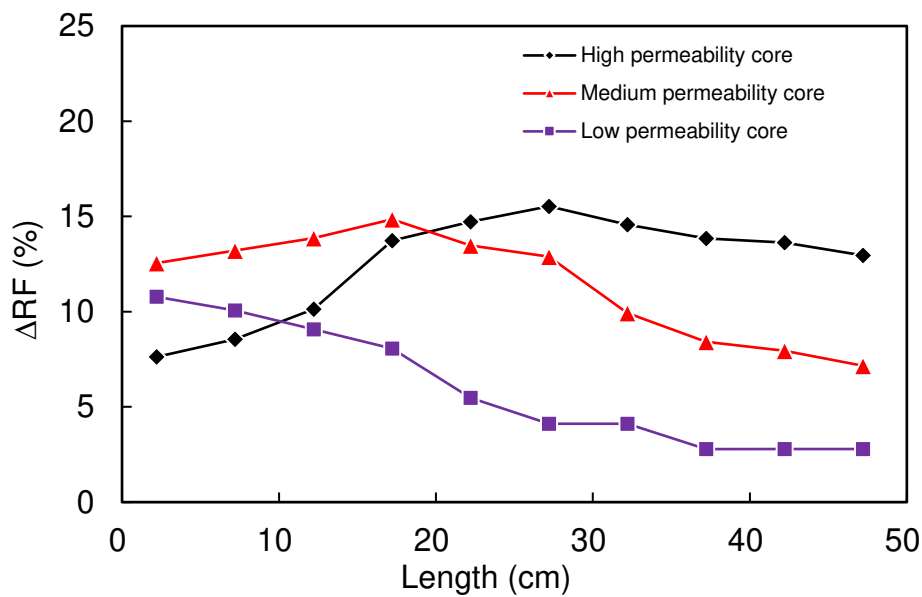
470

471 The distribution of the difference between the final oil RF of the two floods is shown in Figure  
 472 9. The parameter  $\Delta RF$  ( $\Delta RF(\%) = RF(SAG) - RF(CO_2)$ ) represents the degree of improved oil



473 production of SAG flooding compared to conventional CO<sub>2</sub> flooding. For the high permeability  
 474 long core, the improvement in oil production along the injection direction gradually increases,  
 475 reaches a maximum value in the middle ( $L = 27$  cm), and then slightly decreases. The  
 476 improvement in RF that occurs during the soaking stage is controlled by several factors, (i) the  
 477 amount of residual oil at the start of the soaking phase, and (ii) the amount and distribution of  
 478 CO<sub>2</sub> retained in the pores at the beginning of the soaking.

479



480

481 **Figure 9.** The difference in oil RF between the flooding processes as a function of length  
 482 along the cores.

483

484 Proximally to the injection end, there is a larger saturation of retained CO<sub>2</sub>, but production from  
 485 this zone has been good (at least for the high permeability core), so there is only a small amount  
 486 of residual oil. Consequently, there is less scope for the soaking process to be effective, which  
 487 leads to values of  $\Delta RF = 7.62\%$  for the high permeability core. However, more residual oil is  
 488 present for the low and medium permeability cores, which results in a larger improvement in  
 489 recovery factor ( $\Delta RF = 12.55\%$ ,  $\Delta RF = 10.78\%$ , respectively); the medium permeability core  
 490 performing better than the low permeability core because it allows access to more CO<sub>2</sub>.

491

492 The amount of residual oil at the start of the soaking phase gradually increases along the  
493 injection direction, but the amount of CO<sub>2</sub> retained at the beginning of soaking gradually  
494 decreases. Consequently, the central portions of the high and medium permeability long cores  
495 provide the best oil production enhancement and hence the greatest ΔRF (about 14.85% and  
496 15.53%, respectively). The low permeability core does not exhibit this behaviour because its  
497 low permeability reflects the fact that its pores are sufficiently small that even though a large  
498 saturation of residual oil is retained after initial flooding, there is little invasion of CO<sub>2</sub> to enable  
499 much of it to be produced after soaking.

500

501 The values of ΔRF fall again towards the output end of each long core, reflecting that although  
502 the retained oil saturation is high, the CO<sub>2</sub> saturation is low. It is here that there is the greatest  
503 difference between the three different permeability long cores, with the greatest improvement  
504 occurring for the high permeability long core (ΔRF=12.96%).

505

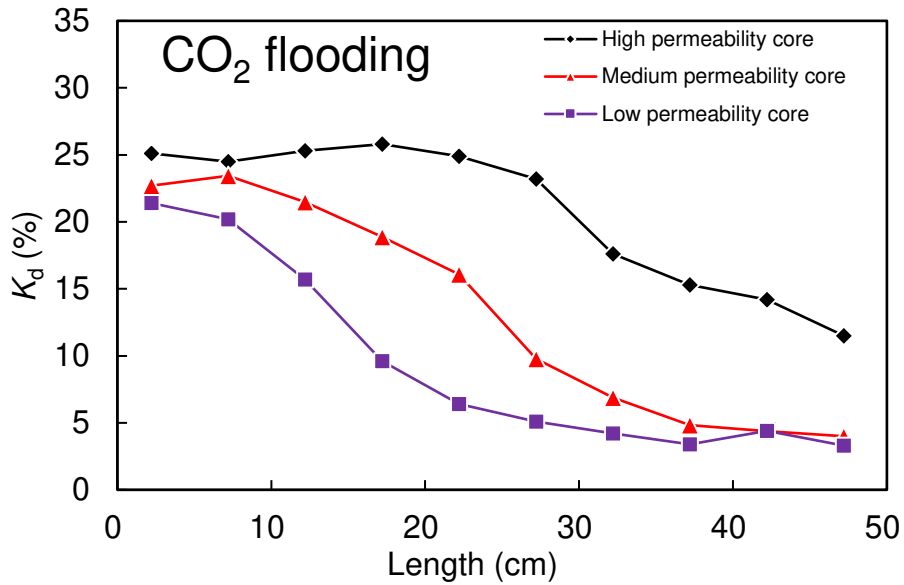
506 In summary, the soaking stage leads to an overall improvement in the recovery factor for cores  
507 of all permeability and at all locations, but the best improvements were in the middle of the  
508 medium and high permeability cores (around 15%) and proximally to the injection end of the  
509 low and medium permeability cores (around 12%).

510

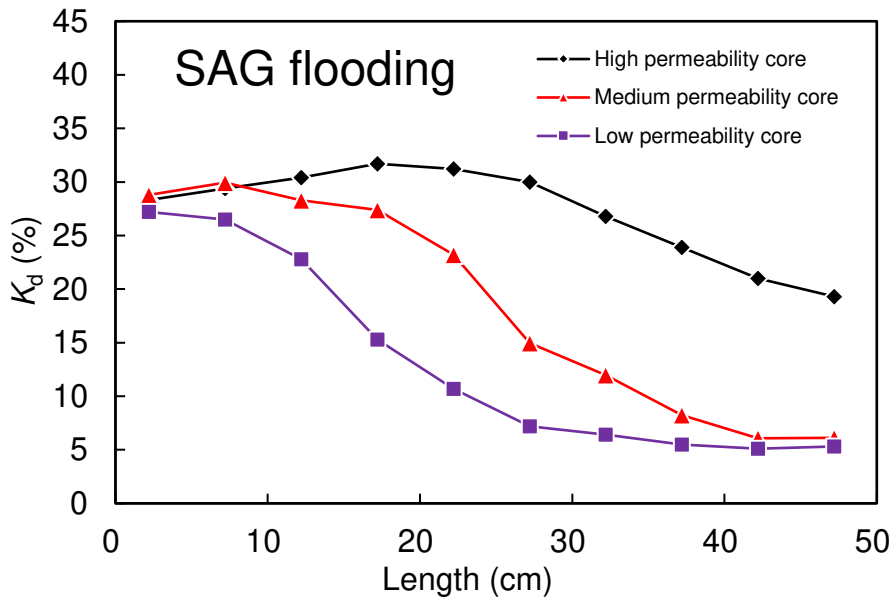
#### 511 Permeability damage

512 We defined a permeability decline parameter as  $K_d$  after flooding ( $K_d = 100 \times (K_b - K_a) / K_b$ , which  
513 is reported as a percentage, and where  $K_b$  is the pre-flooding permeability of the core and  $K_a$  is  
514 permeability of the core after flooding, Figure 10 ).

515



516



517

518 **Figure 10.** The spatial distribution of the reduction in permeability along the cores due to  
 519 precipitation of asphaltene.

520

521 It would be expected that permeability decline is associated with the precipitation of asphaltene  
 522 which reduces the water wettability of the rock as well as blocking flow pathways . It has been  
 523 hypothesized<sup>[10]</sup> that the amount of permeability reduction is controlled by (i) the extent of the  
 524 precipitation of asphaltene, (ii) the efficiency of asphaltene particle migration (initial  
 525 permeability of the rock which depends on its pore microstructure), and (iii) the efficiency with

526 which such particles can block pore-throats. We also recognize that cores and reservoir  
527 formations with higher oil recovery factors have, hosted the passage of more CO<sub>2</sub> during initial  
528 flooding. It would therefore be expected that these rocks would be more likely to exhibit  
529 increased asphaltene precipitation and hence a greater decline in permeability<sup>[37-38]</sup>.

530

531 After conventional CO<sub>2</sub> flooding, the permeability near the injection end ( $L=0-27$  cm) of the  
532 high permeability long core underwent a reduction of about 25%. Moving more distally from  
533 the injection face, the degree of permeability reduction decreases until it is 11.5% at the output  
534 face (Figure 10 top panel). This pattern of permeability damage is the result of the continuous  
535 advancement of the CO<sub>2</sub> flooding front, the continuous solution of CO<sub>2</sub> in the crude oil, the  
536 consequent formation, precipitation and migration of asphaltene particles, followed by the  
537 adsorption of asphaltene onto grain surfaces and their blockage of pore throats.

538

539 The permeability decline of the medium and low permeability long core follows a similar  
540 pattern, but undergoes a slightly smaller permeability reduction at the injection end (about 23%  
541 for  $L=0-7.5$  cm), but then steadily declines until the permeability reduction only about 4% at  
542 the output face.

543

544 It is clear from Figure 10 that CO<sub>2</sub>-SAG flooding causes greater damage to permeability than  
545 conventional miscible CO<sub>2</sub> flooding for all positions along all three cores. The SAG flooding  
546 process provides a similar pattern of permeability reduction for all locations in all three long  
547 cores. This is because during the soaking process larger amounts of CO<sub>2</sub> are dissolved in the  
548 residual oil, which leads to a concomitant increase in asphaltene precipitation, and which then  
549 narrows and blocks pore throats more effectively<sup>[35-36]</sup>. This view is supported by the decrease  
550 in the amount of asphaltene in the produced oil compared to that in the initial oil (Figure 7).  
551 Previously<sup>[10]</sup> it has been noted that, the pattern of permeability decline along the cores was  
552 smoother for CO<sub>2</sub>-SAG flooding compared to CO<sub>2</sub> flooding, and this has been associated with  
553 the soaking leading to a more homogeneous precipitation of asphaltene.

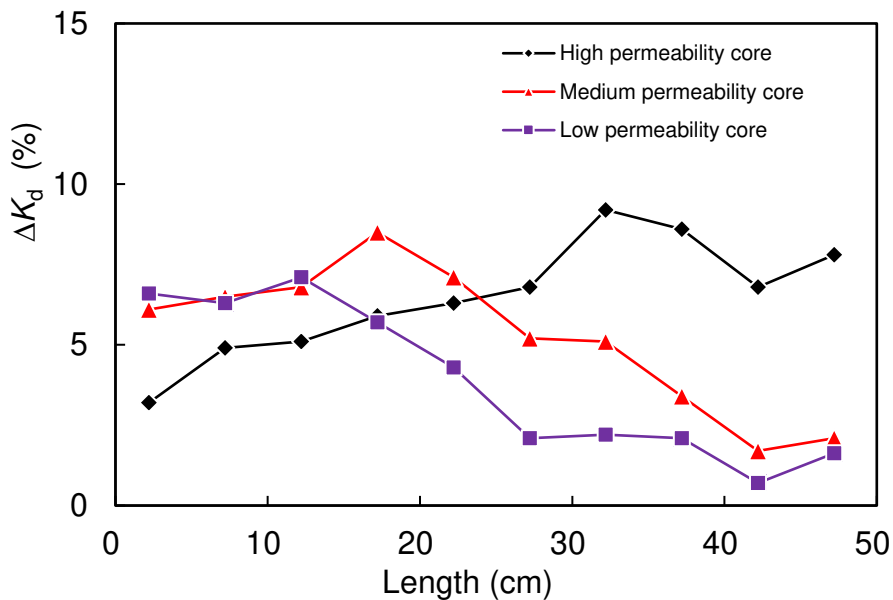
554

555 It is possible to quantify the percentage difference in  $K_d$  between the two flooding processes<sup>[10]</sup>  
556 using  $\Delta K_d(\%) = K_d(\text{SAG}) - K_d(\text{CO}_2)$ , which is shown in Figure 11.

557

558 The  $\Delta K_d$  value in the high permeability layer increases in the direction of injection. The closer  
559 to the outlet end, the more residual oil at  $\text{CO}_2$  BT. Compared with  $\text{CO}_2$  flooding, the additional  
560 precipitation of asphaltene associated with the soaking stage of the  $\text{CO}_2$ -SAG process is greater,  
561 and the asphaltene precipitation during the secondary flooding process has a relatively large  
562 impact on the core permeability at the outlet end.

563



564

565 **Figure 11.** The difference in permeability decline ( $\Delta K_d$ ) between the two flooding processes.

566

567 The distribution trend of  $\Delta K_d$  in the low and medium permeability long cores decreases along  
568 the injection direction, which is exactly the opposite of the trend of  $\Delta K_d$  distribution in the high  
569 permeability long core. This also suggests that interaction of  $\text{CO}_2$  and oil during the soaking  
570 stage occurs mainly in the pores swept and affected by injected  $\text{CO}_2$  before  $\text{CO}_2$  BT, that is, in  
571 the core near the injection end in low and medium permeability long cores. The processes of

572 CO<sub>2</sub> soaking and secondary flooding increased the permeability decline of these cores, and did  
573 not have a substantial influence on the reduction in the permeability of the cores near their  
574 outlet end.

575

576 The  $\Delta K_d$  of the cores proximal to the injection face in the medium and low permeability cores  
577 is higher than the  $\Delta K_d$  near the injection face of the high permeability long core. The significant  
578 additional permeability decline near the injection face in the low permeability core is worthy  
579 of attention, and corresponding measures should be taken at the corresponding injection well  
580 during the SAG flooding process. It shows that CO<sub>2</sub> soaking and secondary flooding has a  
581 substantial influence on the permeability decline of the injection end and middle in medium  
582 permeability long core, while only affects  $\Delta K_d$  at the injection end in low permeability. It also  
583 shows that the CO<sub>2</sub> soaking and secondary flooding have a weak propulsion effect on the  
584 displacement front, but it significantly increases the permeability decline of the cores that has  
585 been swept by CO<sub>2</sub> at CO<sub>2</sub> BT. In short, the distribution characteristics of  $\Delta K_d$  and  $\Delta RF$  are  
586 basically similar.

587

588 In this work we confirm the earlier observation<sup>[10]</sup> that CO<sub>2</sub>-SAG flooding produces greater  
589 permeability damage and a higher oil recovery factor than simple miscible CO<sub>2</sub> flooding. As  
590 before<sup>[10]</sup>, we have used a single parameter ( $K_{dp}$ ) to take account of both oil recovery  
591 improvement and permeability damage. Here,  $K_{dp} = K_d/RF$  measures the amount of  
592 permeability decrease, or damage, per unit increase recovery factor, and is shown for both  
593 flooding processes in Figure 12.

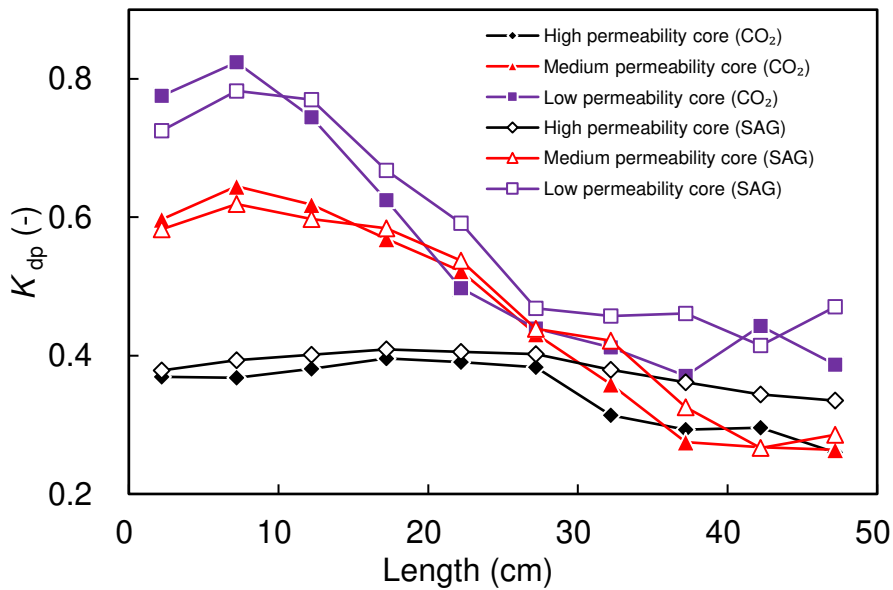
594

595 The  $K_{dp}$  value of the high permeability core is the smallest, and the  $K_{dp}$  value of the low  
596 permeability long core is the largest. This indicates that the large permeability not only leads  
597 to high oil recovery, but also weakens the decline in permeability resulting from precipitation  
598 of asphaltene. It is clear that high initial permeabilities are relatively insensitive to permeability  
599 decline caused by both adsorption of asphaltene precipitation and blockage of pore throats by

600 asphaltene particles. The value of  $K_{dp}$  in the high permeability core changes only slightly along  
 601 the injection direction, while its value shows a marked decrease in the flow direction for the  
 602 low and medium permeability cores.

603  
 604 These observations arise because the gasflood front has advanced as far as the outlet face in the  
 605 high permeability long core but has only advanced partially along the other two cores even  
 606 though viscous fingering ensures that breakthrough has occurred. The value of  $K_{dp}$  falls rapidly  
 607 in the vicinity of the flood front, which occurs at approximately  $20 \pm 7$  cm and  $27 \pm 7$  cm for the  
 608 low and medium permeability cores, respectively. As a consequence, it may be said that  
 609 although some oil is produced from the injection end of the low and medium permeability long  
 610 core, damage to the core permeability is more significant than for the high permeability core.

611



612

613 **Figure 12.** The distribution of the  $K_{dp}$  value along cores after flooding. The  $K_{dp}$  parameter  
 614 represents the percentage permeability decline per unit increase in recovery factor, and for  
 615 which large values are worse than small values.

616

617 In the high permeability long core, the difference in  $K_{dp}$  after CO<sub>2</sub> flooding and SAG flooding  
 618 only exists in the cores near the outlet end, which shows that although the CO<sub>2</sub> soaking and

619 secondary flooding at the outlet end have effectively improved the oil production effect, they  
620 have caused relatively greater damage to permeability. Also, compared with CO<sub>2</sub> flooding, the  
621 improvement in oil production of SAG flooding in the middle cores is less than the damage to  
622 permeability.

623

#### 624 Blockage and adsorption of asphaltene precipitation

625 The permeability decline due to adsorption and blockage effects of asphaltene precipitation can  
626 be separated in order to calculate the two kinds of decline percentage values through cleaning  
627 and flooding after the flooding experiments using special solvent (the cleaning process and  
628 calculation are shown in the “Post-flooding tests” section)<sup>[39]</sup>.

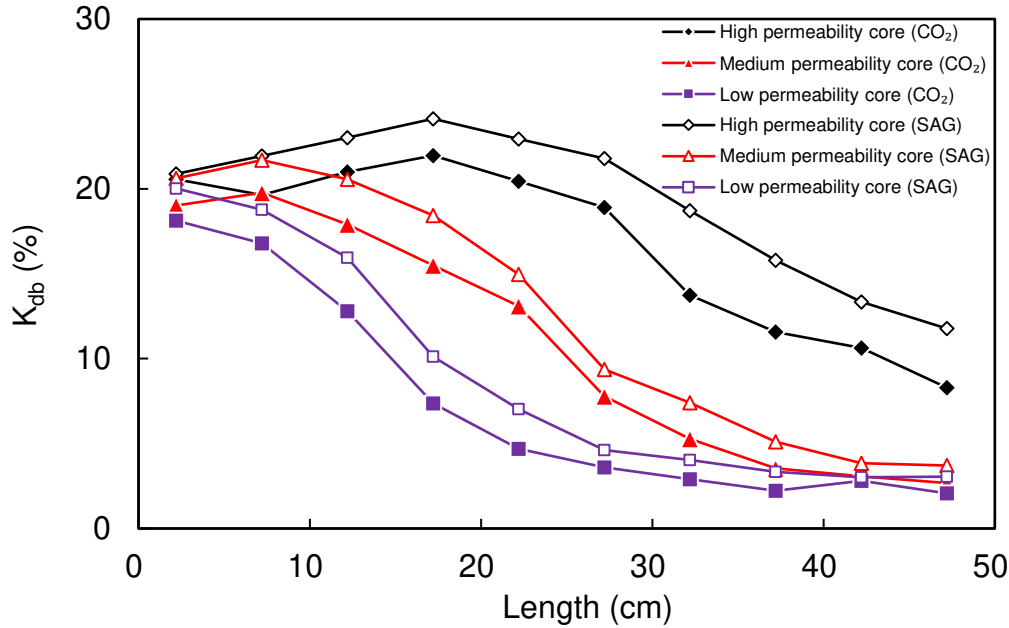
629

630 Figure 13 shows the decrease in permeability caused by asphaltene precipitation blockage of  
631 pore throats after flooding ( $K_{db}=100\times(K_{abc} - K_a)/ K_b$ ), where  $K_{abc}$  is the permeability after the  
632 sample has only been cleaned of blockages. The parameter  $K_{da}$  is the decrease in permeability  
633 caused by asphaltene precipitation adsorption ( $K_{da}=100\times(K_{afc} - K_{abc})/ K_b$ ), where  $K_{afc}$  is the  
634 permeability after the sample has been fully cleaned of blockages and adsorbed precipitation.

635 It will be noted that  $K_d= K_{db}+K_{da}$ . In addition, we define  $R_b=100\times K_{db}/K_d$ , which represents the  
636 percentage of permeability decline caused by asphaltene particle blockage with respect to the  
637 total permeability decline (Figure 14). Here,  $R_a=100-R_b$  is the fractional decrease in  
638 permeability caused by the adsorption of asphaltene with respect to the total permeability  
639 decline.

640





641  
 642 **Figure 13.** The distribution of the reduction in permeability due to asphaltene pore blocking  
 643 along cores after flooding, quantified by  $K_{db}$ , where small values represent small effects from  
 644 the pore blocking mechanism.

645

646 It is commonly considered<sup>[40-41]</sup> that the degree of asphaltene precipitation required to block  
 647 pore throats is related (i) to the overall extent of asphaltene precipitation, (iii) the asphaltene  
 648 particle size distribution, and (iii) the asphaltene particle mobility, all of which are inter-  
 649 dependent. The longer the migration distance of the fluid carrying asphaltene precipitation in  
 650 the pore throats, the greater its velocity, the longer the flooding time, the smaller the size of the  
 651 pore throats, and the more fluid that flows through the pore throat, the higher probability the  
 652 pore throat will be blocked, the more serious the blockage will be<sup>[42]</sup>. However, in the same  
 653 core, the permeability decline caused by asphaltene precipitation adsorption is only related to  
 654 the scale of asphaltene precipitation. Moreover, small particles have less ability to block pore  
 655 throats, but are very mobile (Stokes law), while large particles block pores throats easily but  
 656 are less mobile<sup>[43]</sup>.

657

658 Figure 13 shows that the fall of permeability caused by the asphaltene particle blockage in each  
 659 layer at the injection end is similar. The high permeability core has low resistance to CO<sub>2</sub> flow

660 resulting in more CO<sub>2</sub> being injected, which in turn leads to the deposition of more asphaltenes.  
661 Hence, it would be expected that the permeability decline caused by blockage should be greater  
662 for this high permeability core than the other cores, which is not observed. It is possible that  
663 the initial large permeability of the rock protects it from permeability damage even if there is a  
664 greater deposition of asphaltene<sup>[6]</sup>. By contrast, the lower permeability cores flow less CO<sub>2</sub> and  
665 hence less asphaltene is deposited. However, the asphaltene has a greater potential to cause  
666 permeability decline because the pathways for fluid flow are smaller and less well connected.  
667 Hence, the similarity in  $K_{db}$  between all cores near the injection face is simply due to the  
668 proportionality between initial permeability and the potential for damage which that  
669 permeability provides through asphaltene precipitation.

670

671 In the high permeability long core,  $K_{db}$  gradually increases along the injection direction, and  
672 then drops rapidly after reaching its maximum in the middle of the core ( $L=17$  cm), and finally  
673 the value at the outlet end is smaller than at the inlet end. One possible reason for this is that  
674 the CO<sub>2</sub> injected at the injection end and the middle part interacts with the crude oil to a greater  
675 extent, resulting in a large amount of asphaltene precipitation, which is continuously captured  
676 and accumulated during the migration of the fluid, blocking or reducing pores and throats, and  
677 which then accelerates the capture of asphaltene precipitation particles. Consequently, the  
678 asphaltene precipitation trapped by the pore throats accumulates in a large amount in the middle  
679 of the long cores. The amount of asphaltene precipitation along the injection direction becomes  
680 progressively less, and the  $K_{db}$  value also becomes smaller. The value of  $K_{db}$  after the CO<sub>2</sub>-  
681 SAG process is higher than that after miscible CO<sub>2</sub> flooding. The CO<sub>2</sub> soaking produces more  
682 asphaltene precipitation, and the secondary flooding increases the movement of the fluid  
683 carrying the asphaltene precipitation, enhancing the filtration of the asphaltene precipitation in  
684 the fluid by the pore throats. The value of  $K_{db}$  in the low and medium permeability long cores  
685 decreases continuously along the injection direction, and the  $K_{db}$  value of the low permeability  
686 layer decreases rapidly. this is also due to the position of the displacement front that determines  
687 the distribution of  $K_{db}$ .

688

689 The  $K_{db}$  values at the middle of the three long cores are quite different, while the  $K_{db}$  values of  
690 the middle and low permeability long cores at the outlet end are similar, but are different from  
691 those values for the high permeability long core. The distribution of  $K_{db}$  at the middle and outlet  
692 is similar to that of  $K_d$ . This is also due to the position of the  $CO_2$  flooding front in the medium  
693 and low permeability layers. It also shows that blockage is the dominant factor in determining  
694  $K_d$  in the middle of the long cores and at their outlets.

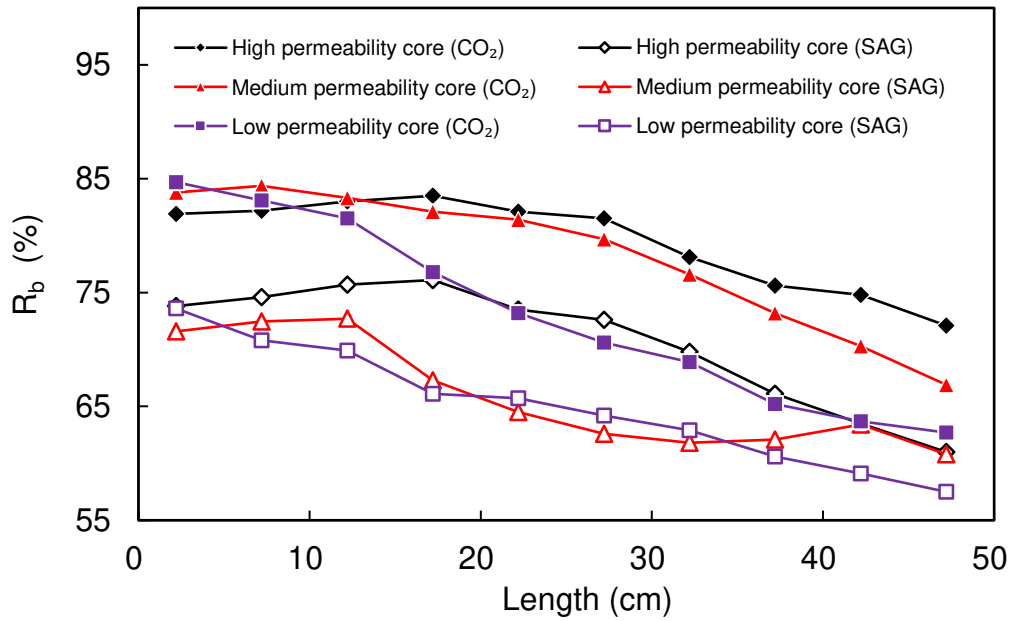
695

696 In addition, there is a certain difference in  $K_{db}$  at the inlet end of the low and medium  
697 permeability layers after  $CO_2$ -SAG and miscible  $CO_2$  flooding, indicating that  $CO_2$  soaking and  
698 secondary flooding increase the degree of asphaltene precipitation to block pores. At the outlet  
699 end,  $CO_2$  soaking and secondary displacement have little effect on the degree of asphaltene  
700 precipitation to block pore throats.

701

702 After  $CO_2$  flooding, the  $R_b$  values at the injection end of the three long cores are similar, the  
703 difference between them becoming larger along the core in the direction of flooding (Figure  
704 14). The  $R_b$  of the core at  $L=0-27$  cm in the high permeability long core remains almost  
705 unchanged, and the  $R_b$  value of the cores decreases slowly at  $L=27-50$  cm. However,  $R_b$  in the  
706 low and medium permeability long cores gradually decreases along the injection direction.

707



708

709 **Figure 14.** The distribution along cores after flooding of the amount of permeability  
 710 reduction attributed to pore throat blocking with respect to the total permeability reduction  
 711 and expressed as a percentage,  $R_b$ .

712

713 Although CO<sub>2</sub> BT occurred in the high permeability layer, the flooding front advanced to the  
 714 outlet end. However, compared with the cores at the injection end and the middle, the  
 715 interaction between crude oil and CO<sub>2</sub> at the outlet end is not so strong, and the pores swept by  
 716 CO<sub>2</sub> are also fewer. In the low and medium permeability long cores, the locations near the outlet  
 717 end are not even swept by CO<sub>2</sub>. It seems that the sweeping and flooding of CO<sub>2</sub> is the key factor  
 718 for pore throat blockage by asphaltene precipitation. It is possible that the complex two phase  
 719 flow of oil and gas is more likely to cause pore throat blockage instead of causing the adsorption  
 720 of asphaltene. The two phase flow of gas and oil near the outlet end is less than at the injection  
 721 end, hence the influence of asphaltene adsorption on the permeability damage gradually  
 722 increases towards the outlet end of the core<sup>[44]</sup>.

723

724 The  $R_b$  value exhibited by the high permeability long core is the largest of all three. This is  
725 because (i) the injected  $\text{CO}_2$  flows predominantly through this core, (ii) the flow rate in this  
726 core is largest, (iii) the two phase flow of oil and gas is more complex, and (iv) asphaltene  
727 precipitation blockage in this core leads to a higher percentage of permeability decline. In  
728 addition, the  $R_b$  value after SAG flooding is lower than that of  $\text{CO}_2$  flooding. This is due to the  
729 fact that no fluid migration occurs during the soaking stage, and the asphaltenes produced  
730 during the soaking stage reduce the permeability in an adsorbed state.

731

732 After SAG flooding, the  $R_b$  values of the three layers at the injection end are relatively close,  
733 and the  $R_b$  value of the high permeability layer is the largest. The distributions of  $R_b$  in the low  
734 and medium permeability long cores are relatively close, and the difference between the high  
735 and medium permeability long cores in the middle of long cores is larger. After  $\text{CO}_2$  flooding  
736 and SAG flooding, the  $R_b$  distribution trend of the medium permeability layer is quite different,  
737 which indicates that the  $\text{CO}_2$  soaking in the middle of the medium permeability long core has  
738 a greater influence on the adhesion state of asphaltene particles, which leads to an increase in  
739 the proportion of adsorbed asphaltene. It is worth noting that  $K_{db}(\text{SAG}) > K_{db}(\text{CO}_2)$ , however  
740  $R_b(\text{SAG}) < R_b(\text{CO}_2)$

741

742 Regardless of the displacement method, the damage to rock permeability (>55%) caused by  
743 asphaltene precipitation blockage in pore throats is higher than the damage caused by  
744 asphaltene adsorption. This is because pore blockage damages the connectivity between the  
745 pores and pore throats in a targeted manner. By contrast, asphaltene adsorption only reduces  
746 the size of both pores and pore throats wherever the precipitation occurs. While rock  
747 permeability will occur by such a mechanism most of the adsorption has no effect on overall  
748 pore connectivity and that which happens to occur at the site of pore throats closes them only  
749 slowly and often partially, thus retaining much of the previous connectivity<sup>[45]</sup>.

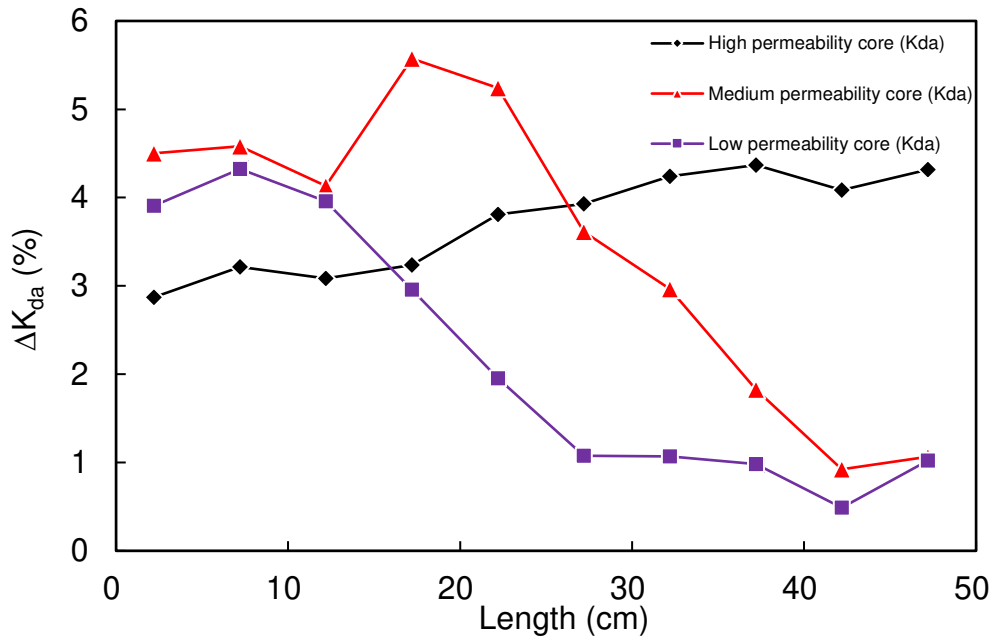
750

751 During the process of recovering the core permeability by cleaning the core of asphaltene  
752 deposits and hence removing pore throat blockages and adsorbed asphaltene precipitation,  
753 which occurred after flooding, it was observed that the asphaltene blocking pore throats was  
754 easier to remove than the adsorbed asphaltene precipitation, the latter of which required a large  
755 volume of solvents for long-term cycle cleaning. It is worth noting that the permeability values  
756 of all core plunger were tested again after being thoroughly cleaned, the permeability of the  
757 same long core at different positions fluctuates less than 3%, and the homogeneity of the long  
758 cores is confirmed.

759

760 The values of  $\Delta K_{da}$  ( $\Delta K_{da} (\%) = K_{da}(SAG) - K_{da}(CO_2)$ ) are the difference in permeability ( $K_{da}$ )  
761 of the layers with the same permeability caused by asphaltene adsorption after the two types of  
762 flooding process. The distributions of  $\Delta K_{da}$  along each of the three long cores are shown in  
763 Figure 15. The  $\Delta K_{da}$  in the high permeability long core gradually increases along the injection  
764 direction, which indicates that compared with  $CO_2$  flooding, the closer to the outlet end, the  
765 stronger the tendency of asphaltene precipitation absorption caused by  $CO_2$  soaking. This is  
766 due to there being more residual oil with higher asphaltene content in the cores near the outlet  
767 end at the beginning of the  $CO_2$  soaking process.

768



769

770 **Figure 15.** The distribution of the difference in the permeability damage caused by asphaltene  
 771 adsorption,  $\Delta K_{da}$  between the two flooding processes.

772

773 However, the distribution trends of  $\Delta K_{da}$  in the low and medium permeability cores are just the  
 774 opposite, showing a downward trend along the injection direction. This pattern is also partially  
 775 the effect of the  $CO_2$  flooding front stays in the cores after  $CO_2$  BT in the high permeability  
 776 long core, which causes  $CO_2$  soaking to increase asphaltene precipitation adsorption at the  
 777 injection end and also towards the middle of the medium and low permeability long core. This  
 778 is also confirmed by the fact that the  $\Delta K_{da}$  of the high-permeability layer at the injection end is  
 779 much larger than that of the low and medium permeability long core.

780

## 781 **Conclusions**

782 Reservoir condition miscible  $CO_2$  flooding and  $CO_2$ -SAG flooding experiments have been  
 783 carried out on 'multilayer' sandstone system. The distributions of differential pressure, residual  
 784 oil, recovery factor and permeability damage by asphaltene precipitation blockage and  
 785 adsorption were quantified. The main findings are summarized below.

786

787 The overall oil recovery factors after CO<sub>2</sub>-SAG flooding for the high, medium and low  
788 permeability long cores, are 7.6%, 8.3%, 7.7% higher than conventional CO<sub>2</sub> flooding. The  
789 fractional oil production of the high, medium and low permeability long cores were 61.6%,  
790 27.7%, 10.6% after CO<sub>2</sub>-SAG flooding, the difference between each layer is less than for  
791 conventional CO<sub>2</sub> flooding.

792

793 The displacement fronts in the low and medium permeability layers are not significantly  
794 advanced due to the soaking stage, which does not significantly expand the sweeping volume,  
795 and only enhances the CO<sub>2</sub> displacement effect in the pores that have been swept by CO<sub>2</sub> before  
796 CO<sub>2</sub> BT.

797

798 After conventional CO<sub>2</sub> flooding, the permeability of the high permeability core near the  
799 injection end has a relatively homogeneous drop distribution by 24.5-25.8%, which is 5.5-  
800 14.3% higher than that of the core near the outlet end, and gradually decreases. The reduction  
801 in permeability for CO<sub>2</sub>-SAG flooding is larger than that for conventional CO<sub>2</sub> flooding.

802

803 The percentage permeability drop caused by asphaltene precipitation blockage is 84.7-62.7%  
804 of the total permeability drop after CO<sub>2</sub> flooding, which represents 5-10% greater decrease in  
805 permeability than that caused by CO<sub>2</sub>-SAG flooding.

806

## 807 **Acknowledgments**

808 Thanks are given to the China Scholarship Council for funding the opportunity of the lead  
809 author to research at The University of Leeds, UK. This research is supported by National  
810 Natural Science Foundation of China, “The formation mechanism of residual gas and liquid in  
811 coal seam and the geological constraints for effective production” (41872171).

812

## 813 **References**



- 814 (1) Cao, M. and Gu, Y., 2013. Oil recovery mechanisms and asphaltene precipitation  
815 phenomenon in immiscible and miscible CO<sub>2</sub> flooding processes. *Fuel*, 109, pp.157-166.
- 816 (2) Lei, H., Yang, S., Zu, L., Wang, Z. and Li, Y., 2016. Oil recovery performance and CO<sub>2</sub>  
817 storage potential of CO<sub>2</sub> water-alternating-gas injection after continuous CO<sub>2</sub> injection in a  
818 multilayer formation. *Energy & Fuels*, 30(11), pp.8922-8931.
- 819 (3) You, J., Ampomah, W. and Sun, Q., 2020. Development and application of a machine  
820 learning based multi-objective optimization workflow for CO<sub>2</sub>-EOR projects. *Fuel*, 264,  
821 p.116758.
- 822 (4) Wang, L., He, Y., Wang, Q., Liu, M. and Jin, X., 2020. Multiphase flow characteristics and  
823 EOR mechanism of immiscible CO<sub>2</sub> water-alternating-gas injection after continuous CO<sub>2</sub>  
824 injection: A micro-scale visual investigation. *Fuel*, 282, p.118689.
- 825 (5) Qian, K., Yang, S., Dou, H., Wang, Q., Wang, L. and Huang, Y., 2018. Experimental  
826 investigation on microscopic residual oil distribution during CO<sub>2</sub> Huff-and-Puff process in tight  
827 oil reservoirs. *Energies*, 11(10), p. 2843.
- 828 (6) Wang, Q., Yang, S., Lorinczi, P., Glover, P.W. and Lei, H., 2019. Experimental  
829 Investigation of Oil Recovery Performance and Permeability Damage in Multilayer Reservoirs  
830 after CO<sub>2</sub> and Water–Alternating-CO<sub>2</sub> (CO<sub>2</sub>–WAG) Flooding at Miscible Pressures. *Energy &*  
831 *Fuels*, 34(1), 624-636.
- 832 (7) Han, J., Lee, M., Lee, W., Lee, Y. and Sung, W., 2016. Effect of gravity segregation on CO<sub>2</sub>  
833 sequestration and oil production during CO<sub>2</sub> flooding. *Applied energy*, 161, 85-91.
- 834 (8) Chen, X., Li, Y., Tang, X., Huang, Q., Sun, X., Luo, J., 2021. Effect of gravity segregation on  
835 CO<sub>2</sub> flooding under various pressure conditions: Application to CO<sub>2</sub> sequestration and oil  
836 production. *Energy*, 2021, 226, p.120294.
- 837 (9) Khan, M.Y. and Mandal, A., 2021. Improvement of Buckley-Leverett equation and its  
838 solution for gas displacement with viscous fingering and gravity effects at constant pressure for  
839 inclined stratified heterogeneous reservoir. *Fuel*, 285, p.119172.
- 840 (10) Wang, Q., Shen, J., Lorinczi, P., Glover, P., Yang, S. and Chen, H., 2021. Oil production  
841 performance and reservoir damage distribution of miscible CO<sub>2</sub> soaking-alternating-gas (CO<sub>2</sub>-  
842 SAG) flooding in low permeability heterogeneous sandstone reservoirs. *Journal of Petroleum*  
843 *Science and Engineering*, 204, p.108741.
- 844 (11) Zhang, J., Zhang, H.X., Ma, L.Y., Liu, Y. and Zhang, L., 2020. Performance evaluation  
845 and mechanism with different CO<sub>2</sub> flooding modes in tight oil reservoir with fractures. *Journal*  
846 *of Petroleum Science and Engineering*, p.106950.
- 847 (12) Li, Z. and Gu, Y., 2014. Soaking effect on miscible CO<sub>2</sub> flooding in a tight sandstone  
848 formation. *Fuel*, 134, pp. 659-668.
- 849 (13) Wang, Q., Wang, L., Glover, P. and Lorinczi, P., 2020. Effect of pore-throat microstructure  
850 on miscible CO<sub>2</sub> soaking-alternating-gas (CO<sub>2</sub>-SAG) flooding of tight sandstone  
851 reservoirs. *Energy & Fuels*, 34(8), pp.9450-9462
- 852 (14) Jafari, B., Ghotbi, C., Taghikhani, V. and Shahrabadi, A., 2012. Investigation on  
853 asphaltene deposition mechanisms during CO<sub>2</sub> flooding processes in porous media: a novel  
854 experimental study and a modified model based on multilayer theory for asphaltene  
855 adsorption. *Energy & fuels*, 2012, 26(8), pp.5080-5091.

856 (15) Lei, H., Yang, S., Qian, K., Chen, Y., Li, Y. and Ma, Q., 2015. Experimental investigation  
857 and application of the asphaltene precipitation envelope. *Energy & Fuels*, 29(11), 6920-6927.  
858 (16) Cho, J., Kim, T.H., Chang, N. and Lee, K.S. Effects of asphaltene deposition-derived  
859 formation damage on three-phase hysteretic models for prediction of coupled CO<sub>2</sub> enhanced  
860 oil recovery and storage performance. *Journal of Petroleum Science and Engineering*, 2019,  
861 172, 988-997.  
862 (17) Wang, Q., Yang, S., Glover, P.W., Lorinczi, P., Qian, K. and Wang, L., 2020. Effect of  
863 Pore-Throat Microstructures on Formation Damage during Miscible CO<sub>2</sub> Flooding of Tight  
864 Sandstone Reservoirs. *Energy & Fuels*, 34(4), 4338-4352.  
865 (18) Cui, G., Zhu, L., Zhou, Q., Ren, S. and Wang, J., 2021. Geochemical reactions and their  
866 effect on CO<sub>2</sub> storage efficiency during the whole process of CO<sub>2</sub> EOR and subsequent  
867 storage. *International Journal of Greenhouse Gas Control*, 108, p.103335.  
868 (19) Hematfar, V., Maini, B. and Chen, Z.J., 2018. Experimental investigation of asphaltene  
869 adsorption in porous media due to solvent injection and effects on relative  
870 permeability. *International Journal of Multiphase Flow*, 99, pp.174-185.  
871 (20) Shen, Z. and Sheng, J., 2017. Investigation of asphaltene deposition mechanisms during  
872 CO<sub>2</sub> huff-n-puff injection in Eagle Ford shale. *Petroleum Science and Technology*, 35(20),  
873 pp.1960-1966.(21) Li, Z., 2014. Optimum Timing for CO<sub>2</sub>-EOR After Waterflooding and  
874 Soaking Effect on Miscible CO<sub>2</sub> Flooding in a Tight Sandstone Formation (Doctoral  
875 dissertation, Faculty of Graduate Studies and Research, University of Regina).  
876 (22) Norouzi, H., Rostami, B., Khosravi, M., & Shokri Afra, M. J., 2019. Analysis of secondary  
877 and tertiary high-pressure gas injection at different miscibility conditions: mechanistic  
878 study. *SPE reservoir evaluation & engineering*, 22(01), 150-160.  
879 (23) Mathur, A., Ali, S., Woodland, C., Hudson, K., Barnes, C., Von Gonten, W.D. and  
880 Belanger, C., 2021, July. Using NMR and Steady State Permeability Measurements to Study  
881 Drilling Fluid Invasion Into the Tight Mississippian Ratcliffe Carbonate and Its Impact on Oil  
882 Production. *In SPE/AAPG/SEG Unconventional Resources Technology Conference. OnePetro*.  
883 (24) Liu, G., Jiang, H., Li, J., Wang, M., Chen, F., Ding, S. and Lu, X., 2015. Evaluation of the  
884 performance of polymer gels mixed with asphalt particle as a novel composite profile control  
885 system. *Journal of Industrial and Engineering Chemistry*, 26, pp.309-314.  
886 (25) Abedini, A., Farshid, T. On the CO<sub>2</sub> storage potential of cyclic CO<sub>2</sub> injection process for  
887 enhanced oil recovery. *Fuel*, 2014, 124, 14-27.  
888 (26) Abedini, A., Torabi, F. Oil recovery performance of immiscible and miscible CO<sub>2</sub> huff-  
889 and-puff processes. *Energy & Fuels*, 2014, 28(2), 774-784.  
890 (27) Li, S., Qiao, C., Li, Z. and Hui, Y., 2018. The effect of permeability on supercritical CO<sub>2</sub>  
891 diffusion coefficient and determination of diffusive tortuosity of porous media under reservoir  
892 conditions. *Journal of CO<sub>2</sub> Utilization*, 28, pp.1-14.  
893 (28) Jin F., Chen S., Wei B., Wang, D., Yang, W., Wang, Y., Lu, J., 2021. Visualization of CO<sub>2</sub>  
894 foam generation, propagation and sweep in a complex 2D heterogeneous fracture network. *Fuel*,  
895 302: 121000.

- 896 (29) Cui, G., Wang, Y., Rui, Z., Chen, B., Ren, S. and Zhang, L., 2018. Assessing the combined  
897 influence of fluid-rock interactions on reservoir properties and injectivity during CO<sub>2</sub> storage  
898 in saline aquifers. *Energy*, 155, pp.281-296.
- 899 (30) Nowrouzi, I., Manshad, A.K. and Mohammadi, A.H., 2019. Effects of dissolved carbon  
900 dioxide and ions in water on the dynamic interfacial tension of water and oil in the process of  
901 carbonated smart water injection into oil reservoirs. *Fuel*, 243, pp.569-578.
- 902 (31) Yang, D., Gu, Y. and Tontiwachwuthikul, P., 2008. Wettability determination of the  
903 reservoir brine-reservoir rock system with dissolution of CO<sub>2</sub> at high pressures and elevated  
904 temperatures. *Energy & Fuels*, 22(1), pp.504-509.
- 905 (32) Al-Bayati, D., Saeedi, A., Myers, M., White, C. and Xie, Q., 2019. An Experimental  
906 Investigation of Immiscible- CO<sub>2</sub> -Flooding Efficiency in Sandstone Reservoirs: Influence of  
907 Permeability Heterogeneity. *SPE Reservoir Evaluation & Engineering*, 22(03), pp.990-997.
- 908 (33) Cui, M., Wang, R., Lv, C. and Tang, Y., 2017. Research on microscopic oil displacement  
909 mechanism of CO<sub>2</sub> EOR in extra-high water cut reservoirs. *Journal of Petroleum Science and  
910 Engineering*, 154, pp.315-321.
- 911 (34) Li, S., Wang, Q., Zhang, K. and Li, Z., 2020. Monitoring of CO<sub>2</sub> and CO<sub>2</sub> oil-based foam  
912 flooding processes in fractured low-permeability cores using nuclear magnetic resonance  
913 (NMR). *Fuel*, 263, p.116648.
- 914 (35) Fassihi, R., Turek, E., Honarpour, M. and Fyfe, R., 2020, August. Investigation of  
915 Permeability Impairment Due to Asphaltene Precipitation During Gas Injection EOR in a Major  
916 GoM Field. *In SPE Improved Oil Recovery Conference*. OnePetro.
- 917 (36) Zanganeh, P., Dashti, H. and Ayatollahi, S., 2018. Comparing the effects of CH<sub>4</sub>, CO<sub>2</sub>, and  
918 N<sub>2</sub> injection on asphaltene precipitation and deposition at reservoir condition: A visual and  
919 modeling study. *Fuel*, 217, pp.633-641.
- 920 (37) Abouie, A., Tagavifar, M. and Sepehrnoori, K., 2018, April. Wettability alteration and flow  
921 coupling in gas flooding of asphaltenic reservoirs. *In SPE Improved Oil Recovery Conference*.  
922 OnePetro.
- 923 (38) Glover, P.W.J. and Walker, E., 2008. Grain-size to effective pore-size transformation  
924 derived from electrokinetic theory. *Geophysics*, 74(1), pp. E17-E29.
- 925 (39) Fakher, S. and Imqam, A., 2019. Asphaltene precipitation and deposition during CO<sub>2</sub>  
926 injection in nano shale pore structure and its impact on oil recovery. *Fuel*, 237, pp.1029-1039.
- 927 (40) Kord, S., Mohammadzadeh, O., Miri, R. and Soulgani, B.S., 2014. Further investigation  
928 into the mechanisms of asphaltene deposition and permeability impairment in porous media  
929 using a modified analytical model. *Fuel*, 117, pp.259-268.
- 930 (41) Sim, S.S.K., Okatsu, K., Takabayashi, K. and Fisher, D.B., 2005, October. Asphaltene-  
931 induced formation damage: effect of asphaltene particle size and core permeability. *In SPE  
932 Annual Technical Conference and Exhibition*. OnePetro.
- 933 (42) Minssieux, L., 1997, February. Core damage from crude asphaltene deposition.  
934 *In International Symposium on Oilfield Chemistry*. OnePetro.
- 935 (43) Soulgani, B.S., Tohidi, B., Jamialahmadi, M. and Rashtchian, D., 2011. Modeling  
936 formation damage due to asphaltene deposition in the porous media. *Energy & Fuels*, 25(2),  
937 pp.753-761.

- 938 (44) Nasri, Z. and Dabir, B., 2014. Network modeling of asphaltene deposition during two-  
939 phase flow in carbonate. *Journal of Petroleum Science and Engineering*, 116, pp.124-135.
- 940 (45) Davudov, D. and Moghanloo, R.G., 2019. A new model for permeability impairment due  
941 to asphaltene deposition. *Fuel*, 235, pp.239-248.